Unterschrift des Betreuers

DIPLOMARBEIT

Foam Control and In-line Cell Density Monitoring in a Laboratory-Scale Bioreactor

ausgeführt am Institut für
Verfahrenstechnik, Umwelttechnik und technische Biowissenschaften
der Technischen Universität Wien

unter der Anleitung von

Assoc. Prof. Dipl.-Ing. Dr.nat.techn Oliver Spadiut

Projektass. Dipl.-Ing. Dr.techn. Julian Quehenberger

Dipl.-Ing. Viktor Sedlmayr

durch

Robert Klausser (01225699)

Wien, 07.11.2022

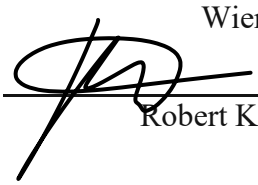

Robert Klausser

Table of Contents

I. Abstract

To design a feasible bioprocess for modern manufacturing a multitude of process parameters must be considered. One of these parameters is the cell density, which is usually aimed to be increased to achieve high space-time-yields. This often results in excessive foaming, which can have disastrous consequences for the fermentation.

Since chemical anti-foaming agents can be detrimental for cell growth and product quality, mechanical solutions for foamy fermentations are demanded. However, commercially designed mechanical foam breakers are not suitable for lab-scale applications due to their spatial and energetic demands. In the first chapter of this thesis, the approach of mechanically breaking foam using an impeller mounted to the main stirrer shaft is critically investigated. 3D-printing is used to prototype and compare different foam breaker designs. We show that this method of defoaming leads to a decrease in bubble size, which stabilizes the foam and can promote foam build-up. Therefore, an alternative approach focussed on foam mitigation is proposed where an alternative submerse impeller configuration is used to keep oxygen transfer high despite reduced agitation and aeration. It is shown that the use of a downward pumping axial impeller close to the surface can improve the volumetric mass transfer coefficient, especially for low agitation and high temperature conditions.

As a determining parameter for the foam build-up, and as a key performance indicator for bioprocesses in general, the concentration of biomass needs to be adequately monitored. In the second chapter of this thesis, we investigate optical and dielectric spectroscopy methods to measure cell density in-line, during continuous cultivations of *Sulfolobus acidocaldarius*. This organism thrives at high temperatures and low pH values. Thus, the performance of three commercially available sensors is examined under these extreme conditions.

II. Acknowledgments

First and foremost, I want to extend my deepest gratitude towards Assoc. Prof. Oliver Spadiut for giving me the opportunity to work on this project. He is one of the most inspiring leaders I have met during my life. Never did I leave a meeting with him, without feeling deeply motivated and ready to meet the next challenge head on.

Thank you for continuing to believe in me!

Furthermore, I want to thank Dr. Julian Quehenberger, for answering any and all questions I've had while working on this thesis. His willingness to explain and teach, as well as his help with experimental planning was invaluable to me.

Thank you for everything I've learnt from you!

I also want to thank the whole IBD group for providing the best work environment I could imagine. Besides being a highly skilled research group, they are a warm and welcoming family.

Thank you all for your kindness!

Special thanks I owe to Dipl.-Ing. Viktor Sedlmayr, for taking me in as his sidekick. Thank you for always taking the time to help me when I asked for it, despite being buried under other projects and students.

But most of all, thank you for being a friend!

I want to heartily thank my parents. It is only due to their endless support, that I am able to write this milestone of my life.

Thank you for your unconditional love and support!

Finally, I want to thank my partner Sonja, who has been accompanying me in one way or another for almost my entire life.

Thank you for being my home when I need it, but also for pushing me out of the front door when I lack the courage to leave on my own!

III. Introduction

III.1 Foaming as a major problem in biotechnology

The problem of excessive foaming is as old as biotechnology itself. Almost a hundred years ago, Buswell and Strickholm investigated large digestion tanks that purified sewage through sedimentation and microbial digestion, which seemed to overflow during summer [1]. When they analysed the contents of the gasses produced by the tanks, they found a significant increase in CO_2 content compared to samples taken during colder times. Clearly the higher temperatures in the summertime had led to an increased microbial activity, which caused a foamy broth and higher gas production, eventually overflowing the digestor.

With the rise of biotechnological production, improving the space-time-yields of bioprocesses became a main objective. High growth rates and cell densities were accompanied by a higher demand for oxygen, which was mainly achieved by increasing agitation and aeration in fermenters. This further contributed to foaminess and the additional parameters complicated the matter. Thus defoaming fermentation systems became a discussed topic in biotechnology literature [2, 3].

While many solutions of chemical and mechanical nature have been developed, they cannot all be employed effectively in every situation. Chemical anti-foams may be harmful for the host organism or cause problems for the downstream unit operations [4]. Mechanical solutions are less effective and not available for every scale and reactor type [5]. This can lead to foaminess being a limiting factor for an otherwise well optimized process. However, the complexity of the gas-liquid interfacial system combined with the diversity of contributors towards foam build-up, means that the problem is often tackled quite cursory. Either chemical anti-foaming agents are added until foaming stops, or lower cell densities are simply accepted.

III.2 An introduction to the mechanics of foam

In the most general terms, biotechnologically relevant foams can be described as a dispersion of a gaseous phase within an aqueous liquid phase. Between the individual gas bubbles, a thin layer of the continuous liquid phase is separating the two interfacial surfaces. When three or more bubbles meet, so called plateau borders are formed, which act like channels containing the bulk of the liquid phase [6]. At those plateau borders, the surfaces also show the strongest curvatures (see schematic depiction in Figure 1). It is also important to note, that emulsions of two liquids share many of the mechanistic attributes of foams, and thus the two systems are

often discussed together within the literature [7, 8]. At least on a simplified level, most theories and phenomena are applicable to both systems.

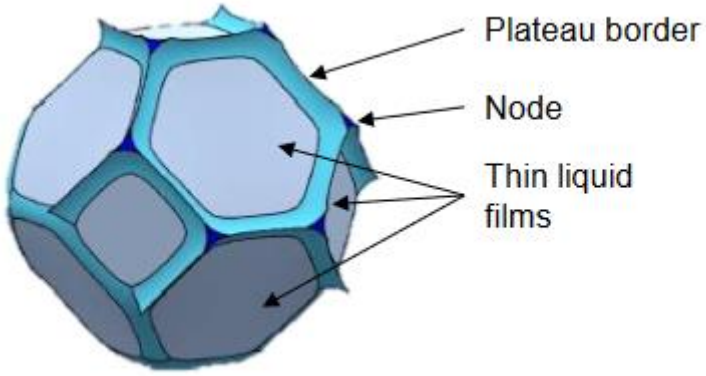

Figure 1: Schematic depiction of a gas bubble within a foam. Most of the interfacial surface area is comprised of thin liquid films while the bulk of liquid phase is contained within the plateau borders. [6]

The requirement for the formation of foams and emulsions is that the interfacial surfaces must be somehow stabilized, to prevent cohesion forces from collapsing the bubble. This can be accomplished by any kind of compound, that tends to adsorb to the interfacial surface. Such compounds are called surface active agents or, more succinctly, surfactants. In many cases surfactants are amphiphilic, which facilitates the adsorption to the liquid-gas interface: the hydrophobic part orientates towards the gaseous phase, while the polar part faces towards the aqueous phase. Similarly, proteins adsorb to interfacial surfaces by arranging their hydrophobic patches and polar groups accordingly. How easily a protein is able to rearrange its tertiary structure ends up being an important factor, determining the provided foam-stabilizing effect [9]. Easier unfolding of the protein causes higher adsorption speeds, which in turn improve foam stability.

Once a cohesive layer of surfactant is adsorbed to the interfacial surface, it is called a monolayer. These adsorbed monolayers, be they protein or another surfactant, weaken the interfacial tension which stabilizes the resulting bubble surface [7]. This effect can be experienced in everyday life, when washing one's hands with soap. Small particles or aggregates are another type of substances that can stabilize the thin layer between two bubbles. However, in this case the stabilization is facilitated by the capillary pressure along the liquid films between individual particles that occupy the bubbles surface [10].

Once the ability of a medium to create foam is given, the stability of the foam determines how much of it is going to build up in a dynamic system like a bioreactor. Several effects have been described that seem to collectively be responsible for the collapse of foam.

III.3 An overview of foam stabilizing effects

Evaporation of the liquid phase will thin out the thin film until the bubble eventually ruptures. The chemical nature of the surfactant influences this process, as denser monolayers produced by substances like fatty alcohols can reduce evaporation [7].

Drainage of the liquid phase is driven by a difference in capillary force between thin films and plateau borders, as well as gravity. Some surfactants prevent drainage by slowing the liquid flow close to the interfacial surface. The literature mentions proteins as an example for this behaviour [8, 11].

Besides evaporation and drainage, bubble coalescence is probably the factor where the strongest influence of surfactants can be observed. After the film between two individual bubbles grows sufficiently thin it will rupture, leaving the sum of gaseous phase behind in a larger (and therefore further destabilized) bubble. Proteins and polymer surfactants are theorized to protect against this mechanism by forming a viscoelastic layer at the interfacial surface [12]. The resulting surface can be stretched farther before it breaks, which also stabilizes the bubbles against rupture by shear forces. Low molecular weight surfactants (LMWS), such as soaps and detergents, stabilize against coalescence due to the Marangoni effect [6, 8, 12]. These smaller molecules form a highly fluid monolayer, in which surfactant concentration gradients can be quickly equalized. This molecular migration creates a flow, that reintroduces liquid phase into the thin film between bubbles. Therefore, the foam stability facilitated by these surfactants is dependent on their fast adsorption and desorption rates. Figure 2 illustrates the differences between LMWS and proteins as surfactants.

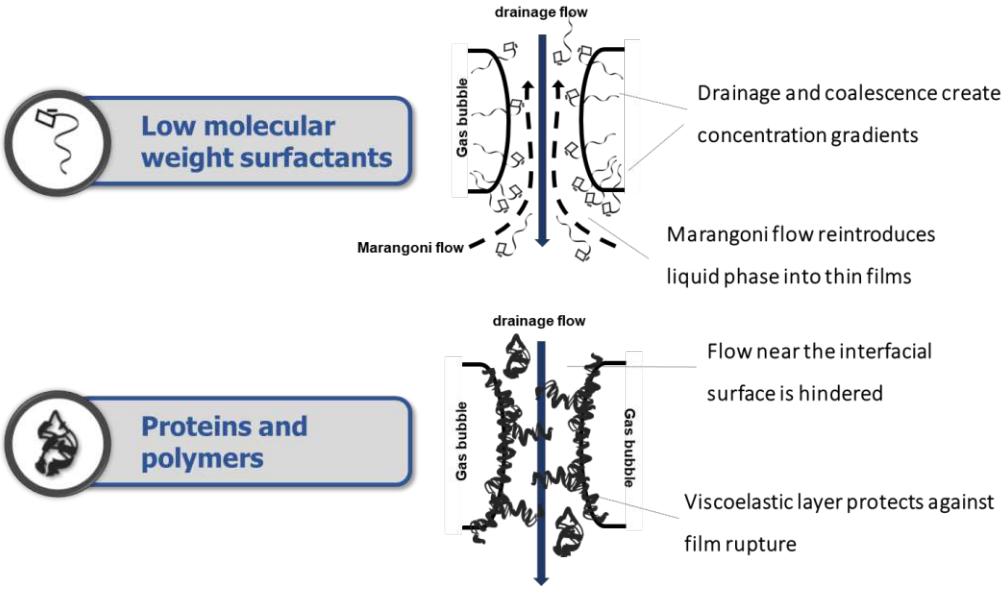

Figure 2: Graphical summary of the different foam stabilizing effects of LMWS and proteins/polymers.

The different foam-stabilizing mechanisms of proteins/polymers and LMWS lead to an interesting trait: a mixture of both types of surfactants produces far less stable foam, than the pure substances would alone. While the larger molecules hinder the flow produced by the Marangoni effect, smaller molecules can move between protein or polymer units and weaken their cohesive intermolecular interactions [12].

Another mechanism of tremendous importance for foam stability is Oswald ripening [6, 10, 13, 14]. This effect is caused by the Laplace pressure inside bubbles. As the curvature along the plateau borders is stronger for smaller bubbles, the applied Laplace pressure inside those bubbles is greater than within larger bubbles. The resulting partial pressure difference between bubbles of varying size imposes a gradient in chemical potential between those bubbles. This causes the diffusion of gas molecules from smaller to larger bubbles. Consequently, the dispersity of bubble size within the initial foam, and the diffusion resistance of the interfacial layer govern the extent of Oswald ripening. A number of interesting observations can be explained by this effect. A foam made by sparging CO_2 through medium will be less stable than one containing N_2, due to the difference in water-solubility between the two gasses [7]. A monodisperse foam will be much more stable than a polydisperse one, due to the smaller differences in Laplace pressure. Long term foam stability can be achieved by stabilisation through larger particles, which is used within the food industry. This was explained and illustrated by Tcholakova et. al. (see Figure 3, [10]) due to the particles forming a densely packed layer at very small bubble sizes. Since the liquid phase between the particles is bent by capillary forces, towards the centre of the bubble, the driving force for Ostwald ripening ceases to exist.

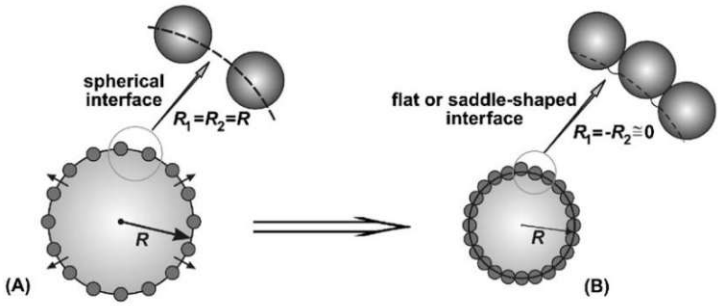

Figure 3: Laplace pressure inside a bubble is negated by a densely packed monolayer of large particles, due to the resulting change in curvature of the interfacial layer. Tcholakova et. at. described this effect as the "arrest of Ostwald ripening". [10]

III.4 Defoaming in biotechnology

While in many fields, such as food science or mineral processing, surfactants are studied with the goal to produce stable foams, in biotechnology foam is usually an unwanted problem to be avoided. Thus evaporation, drainage, and coalescence should be maximized in this context.

Chemical anti-foams are generally considered to be most effective at destabilising foam. These agents induce thin film rupture across every surface within the system at once, thereby leading to extremely fast coalescence. There is a wealth of different anti-foaming agents available, and extensive research on the topic has led to multiple theories regarding their operating mechanisms [15]. While the described modes of action are diverse, and not always entirely understood, there are some generally agreed-upon principles. Most anti-foams consist of hydrophobic and insoluble particles or substances. In the case of particles, they are usually suspended in oils. Once employed, these oils or substances disperse within the aqueous phase. The resulting droplets must be small enough to enter the thin films between individual bubbles, where they can interact with the interfacial system. Oils form a bridge between two neighbouring bubbles, that then continues to stretch out. Either the bridge itself is stretched until it ruptures, or the aqueous film is dewetting from the oil surface until it breaks away [4]. The stretching mechanism is illustrated in Figure 4. Hydrophobic particles act in a similar way, first bridging two gas surfaces, and then dewetting until the aqueous film is completely driven away from the particle and a hole is created [16]. In all cases, anti-foams interact with the interfacial system that is initially stabilized by other surfactants.

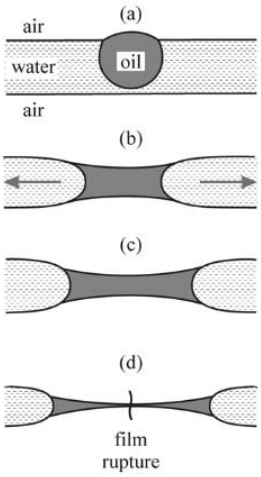

Figure 4: Oil-bridge stretching as described by Denkov and Marinova [17]. An oil droplet forms a bridge between two bubbles (a) that stretches due to imbalanced capillary forces (b). The oil droplet continues thinning (c) until it eventually ruptures (d).

An important disadvantage that results from the enhanced bubble coalescence, is that the available contact surface between gas and liquid is diminished. This results in a decrease in mass transfer between the two phases, a critically important factor for most fermentations. As diffusion through the interfacial surface is the other determining factor for mass transfer, and surfactants and anti-foams strongly interact with these surfaces, it is apparent how foaminess and mass transfer are intrinsically linked.

For this reason, as well as concerns about the biocompatibility of anti-foams, mechanical defoaming has been a topic of interest for many years. While the mechanically induced rupture of foam films is often attributed to a mixture of centrifugal, shear, and impact forces, the exact mechanisms at work are still poorly understood [5, 18, 19]. The simplest foam breaker designs are rotating turbines, discs, or paddles that directly impact the rising foam. The concentration of surfactant seems to have a strong influence on the rotational speed needed to break the resulting foam [19, 20]. As one would expect, higher surfactant concentrations lead to more difficult to break foams. At this point, it should be mentioned that most studies in the field of defoaming are investigating solutions of LMWS. While this makes sense with regards to the reproducibility of such studies, such foams will likely behave differently than the mainly protein stabilized foams in bioprocesses.

Another important insight is that mechanical foam breakers don't entirely separate gaseous and liquid phase like chemical anti-foams. The primary foam, that is produced by agitation and gas sparging through the medium, is broken down into a secondary foam with significantly smaller bubble size. This shift towards more plateau-borders and thicker films results in a foam with a larger volumetric share of liquid phase, thus reducing the overall foam-volume. However, since the interfacial system is now even more stable, the secondary foam cannot be further compacted by the foam breaker [21]. Therefore, successful foam breaking within a closed reactor system necessitates, that more secondary foam is collapsing via coalescence and drainage than produced by breaking the primary foam. It has been shown that spatial separation of the secondary foam into a coalescence column is highly beneficial to achieve mechanical foam control [22].

Further improvements have been made by introducing rotor/stator designs. These force the primary foam through the stator, into interaction with the rotor part. The controlled intake of these designs allow for a well-defined interaction of the foam with the rotor, as well as separation of the secondary foam [23]. Commercially available systems operate similar to centrifuges [24] and cyclones [15]. One such example is shown in Figure 5. However, these

devices require extra motors, sterile couplings into the reactor, and large amounts of space. All of which make these commercial defoaming devices unfeasible for bench scale bioreactors.

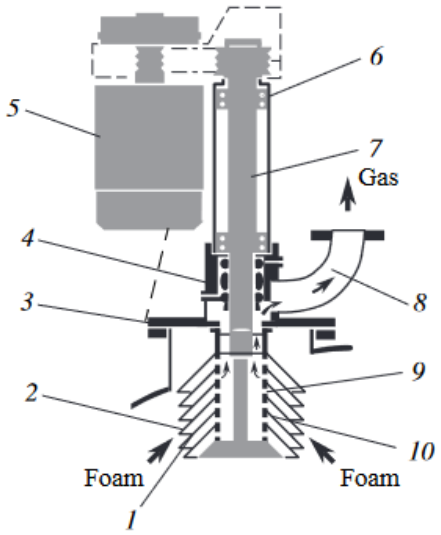

Figure 5: Example of a commercial centrifugal foam breaker as described by A. G. Vetoshkin [24]. The foam is forced through a stack of conic plates (2) separated by radial ribs (1), where the defoaming takes place. The connection to the reactor must be secured through a large flange (3), and a sterile end seal (4). It also requires a large extra gear (5), driving the rotating shaft (7) fixed through a bearing stand (6). While the degassed secondary foam is ejected from the plates back into the vessel, the gaseous phase escapes through gas-passing nozzles (9) and annular barrels (10), towards the gas-bleeding fitting.

As an alternative for small-scale reactors, an extra impeller mounted to the main stirrer shaft is often recommended. Two studies attempting to improve upon this approach were published about 20 years ago [20, 25]. One of them showed successful foam control for a *Saccharomyces cerevisiae* fermentation by implementing the concept. However, in the last decade, little to no studies have been published regarding rotary devices or impellers mounted to the main stirrer shaft.

Instead the discourse on mechanical foam control shifted towards the usage of ultra sound waves [16, 26, 27]. While the data seems promising, and some applications in the food industry are reported [28], no such devices are available yet for the use in lab-scale bioreactors.

III.5 Biomass concentration as a critical process parameter for foam build-up

A high cell density is generally wanted since the biomass either is, contains, or produces the product. As such, biomass concentration certainly is one of the key performance indicators (KPIs) that characterizes an efficient bioprocess [29]. However, within a fermentation system biomass is the primary source of surfactants leading to foam, as cells are the main source of

protein, lipids, and can themselves act as surface-active particles. Due to the devastating effects excessive foaming can have on a bioprocess, the cell density could also be viewed as a critical process parameter (CPP) in this context. In accordance with the initiative towards Industry 4.0, and the implementation of the Quality by Design (QbD [30]) principle for pharmaceutical products, control strategies for such CPPs are demanded [31, 32]. Control in this context refers to continuous measurement and active regulation of the parameter throughout the process. In order to effectively control the CPPs, they must be adequately monitored first. Delayed off-, and at-line analysis often simply does not allow for a timely reaction to influence the parameter. Therefore, QbD hinges on the successful implementation of Process Analytical Technology (PAT) [33]. These analytical tools enable a timely measurement of CPPs, which combined with solid process understanding within the design space [34], lead to continuous quality assurance.

III.6 Measuring biomass concentration in-line

While classical biomass measurements like dry cell weight (DCW) and optical density (OD) are still part of the standard analytical protocol of each fermentation process, these methods are slow, require manual sampling, and can be operator dependent. For these reasons off-line measurements are not suited to reach the goals of automation and process control. Therefore, during the last decades numerous analytical technologies have been developed to measure biomass in-line. Examples include near infrared- (NIR), fluorescence-, RAMAN-, and dielectric spectroscopy, backscatter, as well as soft-sensors [35, 36]. The three methods that were used in this thesis are given a short introduction in the following:

Dielectric spectroscopy is one of the oldest tools for in-line biomass monitoring and has been well established in both industry and research. The measuring principle of the method relies on the electro-chemical properties of cells [37]. Since the outer membrane of cells is essentially non-conductive, but the cytoplasm contains various electrolytes, a cell broth can essentially be viewed as a suspension of tiny capacitors. When an electrical field is applied, each cell contributes to the permittivity measured within the field. However, since a cell's death is usually followed by lysis, only viable cells act as capacitors. Therefore, this method is measuring the viable cell count (VCC). Besides VCC, permittivity measurements have been correlated to the cell specific growth rate, cell morphology, and metabolic state [38]. Since the capacity of the cell suspension is measured, which directly correlates to its dielectric permittivity, dielectric spectroscopy sensors are often called capacity- or permittivity probes.

NIR also has been investigated for biomass monitoring since the previous century [39]. At the energy levels corresponding to the NIR frequency range, vibrational modes of molecules are excited. This leads to absorption of light within this frequency range, which can be measured as a decrease in intensity after transmission through a sample layer of a defined thickness. Alternatively, as light is reflected at particles within the sample, the absorbance can also be measured by analysing the backscattered light [40]. This choice between transmission or reflectance mode is very useful for increasing the dynamic range of measurements. At low cell density there is little light reflected, but the transmission mode is sensitive enough to accurately measure biomass. When the cells grow past the linear range of transmission measurements, the reflective mode becomes useful. This has led to probes that measure "transflectance" [40], combining both modes in one sensor. Another advantage of spectroscopic methods like NIR is that multivariate data can be collected (multiple frequencies). With data analysis methods like principal component analysis (PCA) or partial least square regression (PLS), background effects can be compensated and other components such as metabolites can be analysed [38, 41].

A more recently developed tool for biomass monitoring used during this thesis is the Cell Growth Quantifier (CGQ) by Scientific Bioprocessing (SBI). The CGQ uses LEDs to emit light at 521 nm or 940 nm (depending on the cell density) through a window or glass reactor wall and measures the backscattered light with a photodiode. The intensity of the backscattered light can then be correlated with off-line optical density (OD) or dry cell weight (DCW) measurements [42, 43]. A main advantage of this design is that the sensor is non-intrusive and therefore not influencing the process, as well as being robust against corrosion. However, a resulting disadvantage is that small inconsistencies like scratches in the glass walls introduce inconsistencies between individual fermentations, which necessitates a fine-tuning of the sensor's calibration with off-line data for each new run. Therefore, it could be questioned if the sensors mode of operation can be truly classified as in-line.

III.7 Thesis motivation - *Sulfolobus acidocaldarius*

The topics investigated throughout this thesis were motivated by problems with excessive foaming during a continuous fermentation of *Sulfolobus acidocaldarius*, an aerobic thermoacidophilic crenarchaeon [44].

Wild types of the species *S. acidocaldarius* were first isolated from hot springs in Yellowstone national park [45]. The organism thrives under the extreme conditions of 70 – 75 °C and pH 2.25 – 3.5 [46] and can be cultivated on Vienna Defined Medium [47]. A

key difference to bacteria, which allows *S. acidocaldarius* to thrive under such extreme conditions, are the ether bonds within their membrane lipids [48]. These ether bonds are chemically more stable compared to ester linkages found in bacterial and eukaryotic membrane lipids. Besides diether lipids (DELs), that consist of glycerol-1-phosphate linked to hydrocarbon chains via ether bonds, archaea also produce tetraether lipids (TELs). These TEL's hydrocarbon chains cyclically link two glycerol-1-phosphates, which makes them bipolar lipids [49]. Due to this bipolarity, they can form highly stable monolayer-membranes, that separate two aqueous phases. What makes this especially interesting, is the potential use of archaeal lipids to form archaeosomes [50, 51]. These are liposomes that incorporate archaeal DELs and or TELs, which increases their stability in comparison to conventional liposomes. Besides the use of archaeosomes as a novel drug delivery system, a number of other interesting products and potential applications make the genus *Sulfolobus* an important potential player in the future of biotech [52]: Extremozymes enable enzymatic process steps at high temperatures in food, paper, and textile industry. Sulfolobicins are a class of thermally and chemically stable antibiotic proteins and peptides. Cerchia et. al. used the archaeal chaperonin Ssocpn to build a protein refolding reactor [53].

III.8 Scientific questions

i. **How does a headspace impeller affect excessive foam build-up in a laboratory-scale bioreactor?**

Effective mechanical foam control technologies are only commercially available for larger scale bioreactors. Smaller versions of rotary devices are prevented by the need for additional motors and sterile couplings into the reactor. The logical solution is to simply mount a foam breaker to the existing main stirrer shaft. However, limitations in rotary speed make it difficult to control intense foaming in this way, and studies in the literature have mainly tried to control the foam of low molecular weight surfactants. In this thesis, 3D printing is used to test new foam breaker designs, that may be able to effectively control excessive foam build-up from a real-world fermentation process from our laboratory.

ii. How does a downward pumping axial stirrer close to the surface affect the volumetric mass transfer?

As it has been shown that the mechanical destruction of foam is difficult for heavy foam loads, new approaches may be necessary in cases where anti-foaming agents are not an option. In this thesis, a preventive approach is proposed: To mitigate foaming, agitation and aeration should be kept to a minimum. Since these are also the main process parameters that regulate oxygen transfer, an alternative stirrer configuration is investigated to potentially compensate for the otherwise lowered mass transfer coefficient.

iii. How is the performance of three commercially available in-line biomass sensors affected by harsh conditions like high temperature and low pH?

Accurate prediction of foaminess is a requirement if the foam build-up within a bioreactor is to be controlled via the process parameters. Since surfactant concentration is one of the defining parameters regarding foaming, and the majority of surfactant concentration directly relates to the biomass concentration within a bioreactor, cell density is likely to be a key factor to predict foaminess. As an assortment of commercial probes relying on different physical methods of measuring cell density have recently entered the market, my aim was to test these methods on their applicability for *Sulfolobus acidocaldarius*. This extremophile organism prefers temperatures around 75 °C and a pH of 2 – 3. The performance under such extreme conditions will be compared for three different sensors.

The first two of these questions are answered in the form of a paper draft in chapter A. The third question will be examined within Chapter B of this thesis.

IV. Chapter A – Paper Draft: The Myth of the Headspace Impeller – Foam Control and Improved Mass Transfer via Alternative Stirrer Configuration

IV.1 Abstract

Excessive foaming remains a frequently encountered problem in biotechnology. This is most effectively dealt with by adding chemical anti-foaming agents. However, these agents are often unwanted, and mechanical defoaming devices are not available for the lab-scale. In this work, the frequently recommended alternative of an impeller mounted to the main stirrer shaft of a stirred tank fermenter is investigated in a lab-scale vessel. 3D-printing is used to efficiently build prototypes of novel impeller designs based on the reviewed literature. These designs are tested against foam from a *Sulfolobus acidocaldarius* cell broth, representing a foam stabilized by the typical surfactants found within bioprocesses. It is shown, that due to the reduction of bubble size, a foam breaker mounted to the main stirrer shaft can increase foam build-up instead of reducing it. Hence, an alternative approach focussed on foam mitigation is suggested instead. This approach is based on keeping agitation and aeration to a minimum, while oxygen mass transfer is maintained. To achieve this, a downward pumping axial impeller is used as the upper impeller instead of the typical second Rushton turbine. The influence of this stirrer configuration on oxygen mass transfer is investigated across a range of stirrer speeds, gas flowrates, the upper stirrer position, and at elevated temperatures. It is shown that the volumetric mass transfer coefficient can be significantly increased by this alternative arrangement, thus enabling the use of lower agitation speeds to reduce the foam build-up.

Keywords: defoaming, foam mitigation, mechanical foam breaker, oxygen mass transfer, kLa, axial impeller, segment impeller, thermophiles

IV.2 Introduction

While beer brewers across the world practice their craft to produce a perfect bubbly crown on their beverage, biotechnology has an entirely different relation to foam. During microbial fermentations, excessive foaming is one of the most commonly encountered problems. The

many issues caused by foam overflow, such as the loss of biomass and medium, change in media composition, and blocked exhaust filters, necessitate effective foam control strategies [4, 5]. The most commonly employed strategy to resolve this issue is the use of antifoaming agents. While this approach is able to combat very high loads of foam build-up, it is also often not desired in biomanufacturing for multiple reasons including toxicity to the cultivated cells, reduced mass transfer, and complications during the downstream processing [4, 54].

An interesting example illustrating this restriction is the use of *Sulfolobus acidocaldarius* as production host in industrial bioprocesses. Among other interesting properties [52], this extremophilic crenarchaeon has garnered increasing attention in recent years for its unique membrane lipids, which can be extracted from the biomass [48]. Due to their hydrophobic nature, anti-foaming agents would be extracted alongside those lipids, causing problems during the downstream operations. However, excessive foaming during the cultivation necessitates, that physically based defoaming alternatives are found.

Besides the use of ultra-sonic sound waves [27, 28, 55], most mechanical foam control devices use rapidly spinning rotors to break foam bubbles by applying a combination of shear and centrifugal forces [5, 18, 19]. While such foam breakers are used within the industry, they come with several drawbacks. Contrary to chemical anti-foams, mechanical devices cannot fully defoam a solution, but break down a coarse primary foam into a dense secondary foam [21, 22]. While this significantly lowers the foam volume, the very stable secondary foams cannot be further compacted by the rotor. This is all the more challenging, when ceaseless foam generation during a continuous fermentation is considered. Furthermore, the additional motor required for these foam breakers impose high additional energy costs on the process, and spatial limitations make the commercially available devices unsuitable for lab-scale reactors.

A frequently recommended solution for small fermenters is to mount a rotor to the already existing main stirrer shaft (referred to as a “headspace impeller” in the following). Since no additional motors or mechanical seals are required for the implementation, this method promises minimal additional energy costs, a reduced contamination risk, and easy implementation compared to a large rotary device. While this approach is mentioned in both books and studies on the topic [5, 18, 19, 56], upon extensive review of the literature only two studies trying to optimize the concept were found [20, 25]. These studies highlight a major challenge for headspace impellers: the coupling of agitation and foam breaker speed. Besides mixing, the main purpose of agitation within a bioreactor is to improve the oxygen transfer between gas and liquid phase by dispersing the gaseous phase into smaller bubbles, thereby increasing the exchange area [57]. However, since a reduced bubble size stabilizes foam,

stronger agitation also promotes foam build-up [58]. This leads to a dilemma: attempting to use higher stirrer speeds to improve the foam breaking ability of the headspace impeller also produces a harder to break foam. However, minimizing agitation is opposed by the need of providing sufficient oxygen to the cultivated organism. Nonetheless, Deshpande et. al. still showed a significant increase in foam breaking capability for a few novel impeller designs, conceptualized for this exact purpose [19, 20].

In this work we examine several different headspace impeller designs, that would fit within the constraints of a continuous *S. acidocaldarius* cultivation in a lab-scale vessel. Upon discovering that under these circumstances a headspace impeller seems to be counterproductive, we suggest that mechanical foam control within small reactors should be approached based on mitigation rather than destruction. We show that oxygen mass transfer can be significantly improved by employing an alternative stirrer configuration, allowing for reduced agitation and gas flowrates.

IV.3 Methods and Materials

IV.3.1 Experimental Set-up

All experiments were conducted within a cylindrical glass reactor with an inner diameter of 130 cm and a round bottom. No baffles were used, temperature was measured within a submersed steel tube, and compressed air was fed through a sintered steel micro-sparger at the bottom centre of the reactor. The air-flowrate was controlled via a mass-flow-controller calibrated between 0.10 and 2.00 L/min. The reactor had an inner volume of 3 L and was filled with 2 L of liquid medium for experiments. The bottom stirrer was a Rushton turbine with a diameter of 5.1 cm, which equates to a diameter ratio of 0.4 between impeller and inner vessel diameter. This bottom impeller was always positioned 215 mm from the headplate, which placed it directly above the air-sparger. A schematic drawing of the setup is shown in Figure 6.

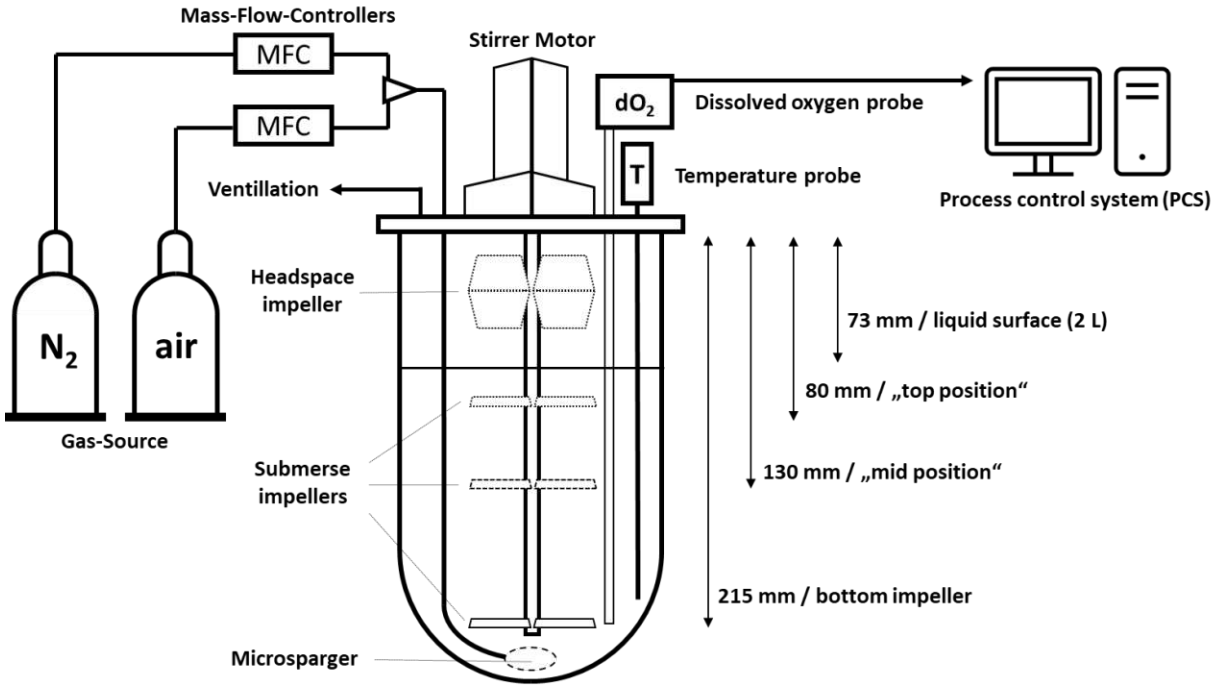

Figure 6: Schematic experimental setup of the lab-scale bioreactor. Usage of the different impeller positions was dependent on the specific experiment and is mentioned when the experiment is discussed. N_2 was only connected for the kLa measurements.

IV.3.2 Headspace Impeller Design

The investigated headspace impellers were designed with the software *Autodesk Fusion 360* and 3D printed using a *Prusa i3 MK3S+*. All impellers were printed from polylactic acid at 0.2 mm printing resolution. The printed impellers were attached to the stirrer shaft by being tightly clamped between two stainless steel rings. The designs are shown in Figure 7.

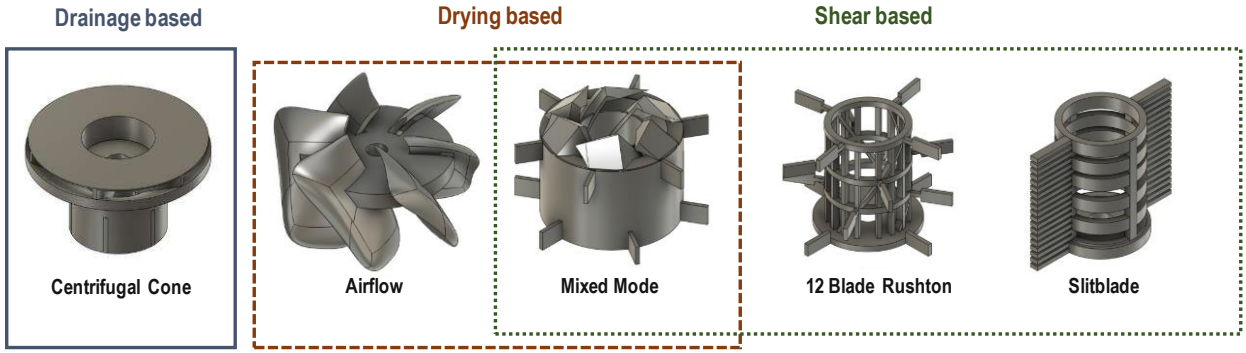

Figure 7: Drawings of the 3D printable headspace impeller designs. They can be grouped according to the foam breaking mechanism that was focussed on with the design. The "Centrifugal Cone" is similar to an inverted hollow spinning cone [59]; The "Airflow" design used large angled paddles designed to produce a downward airflow; The "Mixed Mode" had an inner part fashioned after a turbine to produce downward airflow, as well as Rushton Blades along the outer edges; The "12 Blade Rushton" stacked three rings of 4 Rushton blades; The "Slitblade" is based on the comb design by Deshpande et. al. [20] which showed superior foam breaking capability compared to standard impellers. This version increases the number of cones vertically.

IV.3.3 Foam Experiments

Cell broth of a *S. acidocaldarius* fermentation with $OD_{600} = 25$ was used for the final experiments regarding foam height and overflow. If no active fermentation was available, a solution of 15 g/L skim milk protein was used as a foamy medium substitute for preliminary experiments, as this concentration produced comparable foam to the cell broth (data not shown). Foam heights were measured from the reactor headplate whilst recording videos of the rising foam when analysing overflow-times. During the final comparison between the shear-based designs, no submerse impellers were used to enhance the initial foam bubble size and therefore increase the observable effect on foam stability.

IV.3.4 Measuring the Volumetric Mass Transfer Coefficient

Vienna Defined Medium [47] tempered between 23 - 24 °C (if not stated otherwise) was used for all kLa measurements. Figure 8 shows the dimensions of the Rushton turbine and the downward pumping 3-blade-segment impeller (D3BS) that were compared in the upper impeller positions (the "top position" and "mid position" indicated in Figure 6). Dissolved oxygen (dO_2) was measured using a Hamilton VisiFerm DO Arc Sensor positioned with 1 cm clearance to the reactor wall at the same hight as the bottom impeller. Before measurements, the dO_2 probe was calibrated by first introducing nitrogen until all dissolved oxygen was removed (0 %), and then letting the dissolved oxygen fully equilibrate under the experimental conditions (100 %). kLa was measured using the dynamic gassing-out method [60]: First, dO_2 was set to 0 % by sparging nitrogen through the medium, then the dO_2 signal was recorded with a data collection interval of 6 s until a stable 100 % dO_2 was reached. The volumetric mass transfer coefficient was calculated by numerically approximating the parameters of the equation

$$OTR = kLa \cdot (c_{O2}^{*} - c_{O2}) \tag{1}$$

to fit the measured dO_2 signal and reading out the resulting value for kLa. This was accomplished using a MATLAB script by Julian Kager [61].

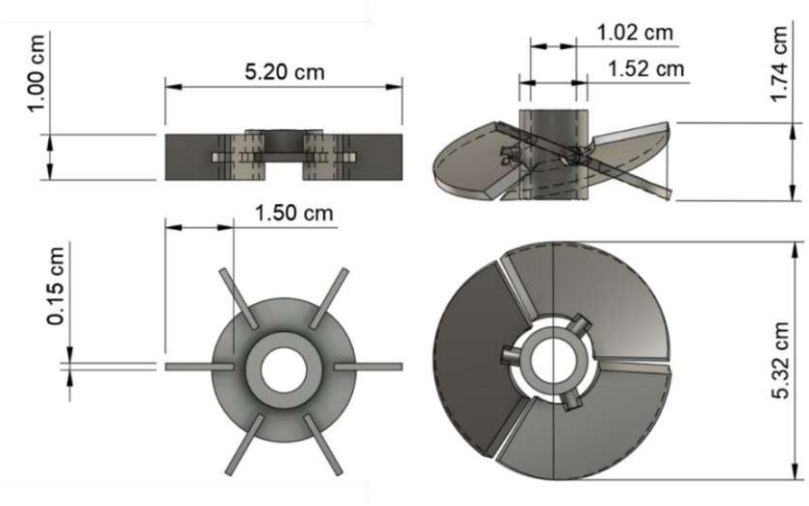

Figure 8: Measurements of the radial pumping Rushton turbine (left) and the axial pumping 3-blade-segment impeller (right).

IV.3.5 Design of Experiment

For the investigated Design of Experiment (DoE), a full factorial design with two quantitative factors (stirrer speed and air flowrate) as well as the qualitative factor of the axial vs. radial impeller type was chosen. The centre treatment was measured in triplicates for each impeller type. The chosen design space included stirrer speeds from 300 - 700 rpm and gas flowrates from 0.15 – 0.35 vvm. For the stirrer type, a 3D printed D3BS impeller was used as an axial stirrer, while a standard stainless steel 6 blade Rushton turbine was used as the radial impeller. Both impellers had an impeller to vessel diameter ratio of 0.4. Both the experimental design, the statistical evaluation, and creation of the resulting model were performed using the software *MODDE 12*. Figure 9 visualizes the investigated design space.

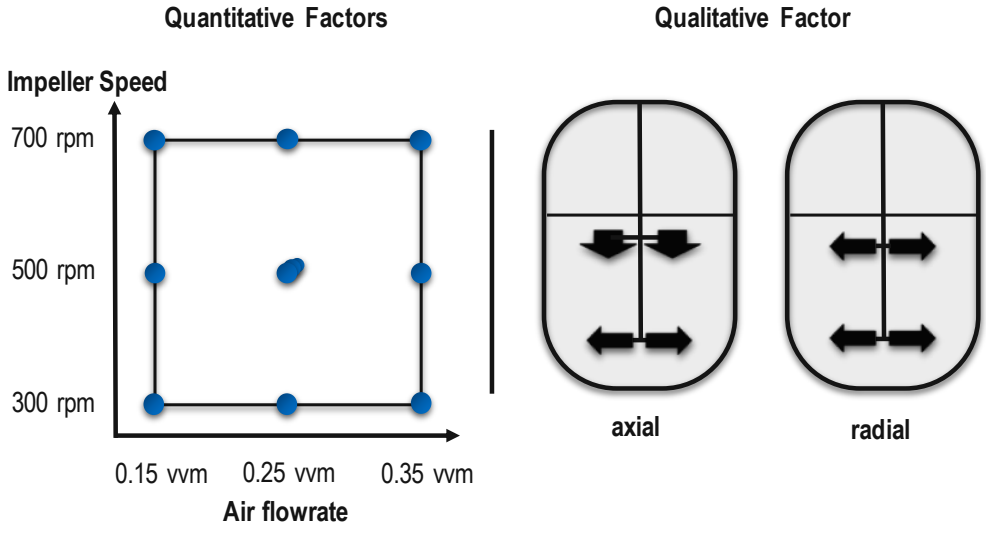

Figure 9: Design space of the DoE investigating the influence of stirring speed and air flowrate combined with either the axial or radial top stirrer.

IV.3.6 Estimation of the specific power input

The specific unaerated power inputs were estimated for the individual impellers with the equation [62]

$$\frac{P_U}{V} = \frac{P_O \cdot N^3 \cdot D^5 \cdot \rho_L}{V} \tag{2}$$

with the power numbers $P_{O,R} = 5$ for the Rushton turbine [62, 63], and $P_{O,D3BS} = 2.1$ for the D3BS impeller [64] found from the literature. Aerated power inputs were estimated via equation (3).

$$\frac{P_G}{V} = \frac{RPD \cdot P_U}{V} \tag{3}$$

By calculating the gas flow number

$$Fl_G = \frac{Q_G}{N \cdot D^3} \tag{4}$$

and the impeller Froude number

$$Fr = \frac{N^2 \cdot D}{g} \tag{5}$$

the expected flow regime for the Rushton impellers was determined to be vortex cavities by looking at the regime flow map depicted within the appendix (Figure 14; Fl_G = 0,011; Fr = 0,186). For vortex cavities a relative power demand of RPD ~ 0.9 was assumed [62].

For the D3BS impeller estimation of RPD was difficult, since no data matching the exact impeller that was used could be found. However, since very similar impellers show no significant change between unaerated and aerated power numbers in the literature [62, 64], RPD = 1 was assumed.

IV.4 Results and Discussion

IV.4.1 Testing headspace impeller designs.

Our impeller designs can be categorized into three groups, corresponding to the foam breaking mechanism they were geared towards: shear force, drainage (by centrifugal force), and drying. The designs aimed at using airflow to dry the foam surface did not seem to impact the foam build-up at all. The limited rotational speeds (200 rpm – 700 rpm) of the main stirrer shaft made it difficult to create a strong air flow within the reactor. Furthermore, fresh air is sparged into the reactor through the medium, which makes the gaseous phase within the reactor headspace already very humid. The humidity preventing film rupture by drying is an effect that also can be seen when cooking noodles in a pot with a lid on. As the lid traps the steam, the foam quickly rises until the pot overflows. However, when the lid is lifted in time, the foam quickly collapses.

A more promising concept in theory was a spinning cone design. Some literature [59, 65] had shown impressive results using spinning inverted cones mounted to the main stirrer shaft. It was postulated, that such rotors mainly destroy foam as it is pumped up along the inner cone surface [5]. However, these works were investigations on large-scale vessels using cone inlet diameters of 25 cm up to 1 m. As spatial limitations from probes and the inner stirrer shaft only allowed for a 3 cm inner diameter in our vessel, we did not see any significant foam intake into the inner cone. It seems likely, that the inlet was simply too small to take up any meaningful amount of foam. Therefore, no suction was created, and the design failed to have a large impact on the foam build-up.

Trying to maximize the shear force created within the reactor headroom seemed to be the most promising design goal for a foam breaker within a small-scale bioreactor. However, when the shear force-based designs were tested, we noticed that the foam build-up got significantly worse compared to not using a headspace impeller at all. To maximize the observable effect of the headspace impellers, an experiment was run under conditions mimicking a “bubble column”. This meant that there were no submerse impellers used while air was simply dispersed into the reactor via a micro sparger, thus increasing the primary foams bubble size. The direct comparison of the foam build-up is shown in Figure 10, or can be seen in a supplemented video. {a video will be linked for a submitted version}

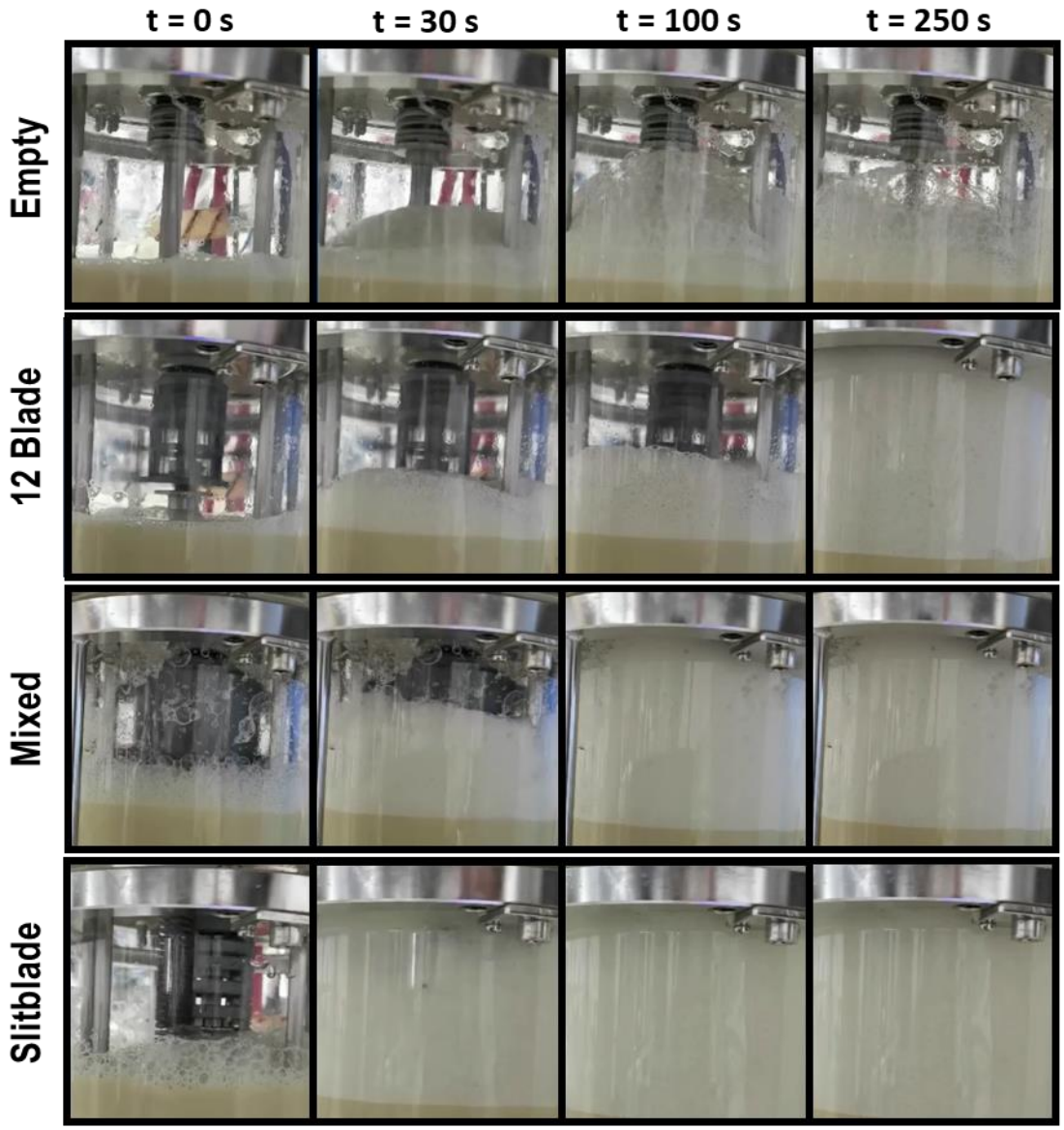

Figure 10: The shear force-based headspace impellers are compared with an empty headroom. The foamy test medium was fermenter broth from a continuous Sulfolobus acidocaldarius cultivation. The shown timepoints are chosen based on the time it took to overflow the reactor. (The "Slitblade" impeller reached overflow at about 30 s, and so on…). A supplementary video of the comparison will be linked within the appendix for a submitted version.

The only configuration that did not lead to the reactor overflowing was not using a headspace impeller at all. Furthermore, impellers that were expected to be more efficient in reducing the bubble size based on the literature also produced a faster overflow. This is most likely due to the increased stability of a foam with a smaller bubble size. While the primary foam within the empty headroom is coarse enough to break on its own, the secondary foam created by the foam breakers is stable enough to accumulate until overflow occurs.

Comparing our results to the findings of Takesono et. al., who did achieve foam control during a cultivation of *Saccharomyces cerevisiae* using a headspace impeller mounted to the main stirrer shaft, there are some notable differences regarding the reactor set-up [25]. Firstly,

they used an impeller with a diameter ratio of 2/3 compared to the vessel's inner diameter. In our reactor the probes installed through the headplate did not allow diameter ratios larger than 1/2. Secondly, they used a stirring speed of 1000 rpm. Our *S. acidocaldarius* cultivations were limited to 700 rpm, due to sensitivity against shear stress at higher agitation speeds. Furthermore, the fermenter in Takesono's study was filled up to 40 % of the reactor's height, while our 2 L working volume amounts to almost 70 % of the reactors volume. Since the secondary foam needs time and space to settle via drainage and coalescence, it can be assumed that purely mechanical foam control requires very large "dead" volumes within the reactor. Some larger designs solve this by separating primary and secondary foam with the addition of a coalescence column [21, 22]. However, the headspace impeller approach does not allow for this separation, and such designs to our knowledge are not available for standard lab-scale fermenters.

Besides the increased stability, the reduction in bubble size within secondary foams also leads to an initial decrease in total foam volume. We believe that this might be the reason for the large amount of anecdotal evidence for headspace impellers. If only a short burst of foam must be compensated, for example at the end of a batch phase, this approach can indeed work as a solution. However, if there is constant foam build-up over a long period of time, such as in a high cell density continuous cultivation, a foam breaker mounted to the main stirrer shaft is most likely a disadvantage.

IV.4.2 kLa influence of an axial top stirrer

Besides the surfactant concentration, agitation and aeration rates are the main contributors towards foam build-up. Therefore, to mitigate foaminess within a stirred tank fermenter, agitation and gas flow must be minimized without failing to meet the oxygen demand of the fermentation. After Van't Ried [60] the oxygen transfer rate (OTR) within a system can be described as

$$OTR = kLa \cdot (c_{O2}^{*} - c_{O2}) \quad (1)$$

with c_{O2}^{*} being the maximum, and c_{O2} the current dissolved oxygen concentration within the liquid phase. Since there is only a limited possibility of influencing c_{O2}^{*}, the volumetric mass transfer coefficient kLa must be improved. While the most effective way of increasing kLa is the reduction of the bubble size by agitation, to mitigate foaming other ways of achieving higher

mass transfer rates are required. We chose to attempt this by exploring an alternative stirrer configuration.

While there is literature that discusses the influence of axial impellers on the kLa [57, 66, 67], there is no definitive consensus on its impact in combination with a Rushton turbine. Owing to the complexity of the matter, this might also be dependent on the specific vessel geometry. After promising preliminary experiments (data not shown), the influence of an axial upper stirrer instead of the typical dual-Rushton combination was investigated using a DoE approach. A contour plot of the resulting model is shown in Figure 11. Both stirring speed and air flowrate seemed to have a linear influence on the mass transfer within the design space. This trend was independent of the employed upper impeller. Comparing the stirrer types, the axial impeller led to a significant increase in kLa.

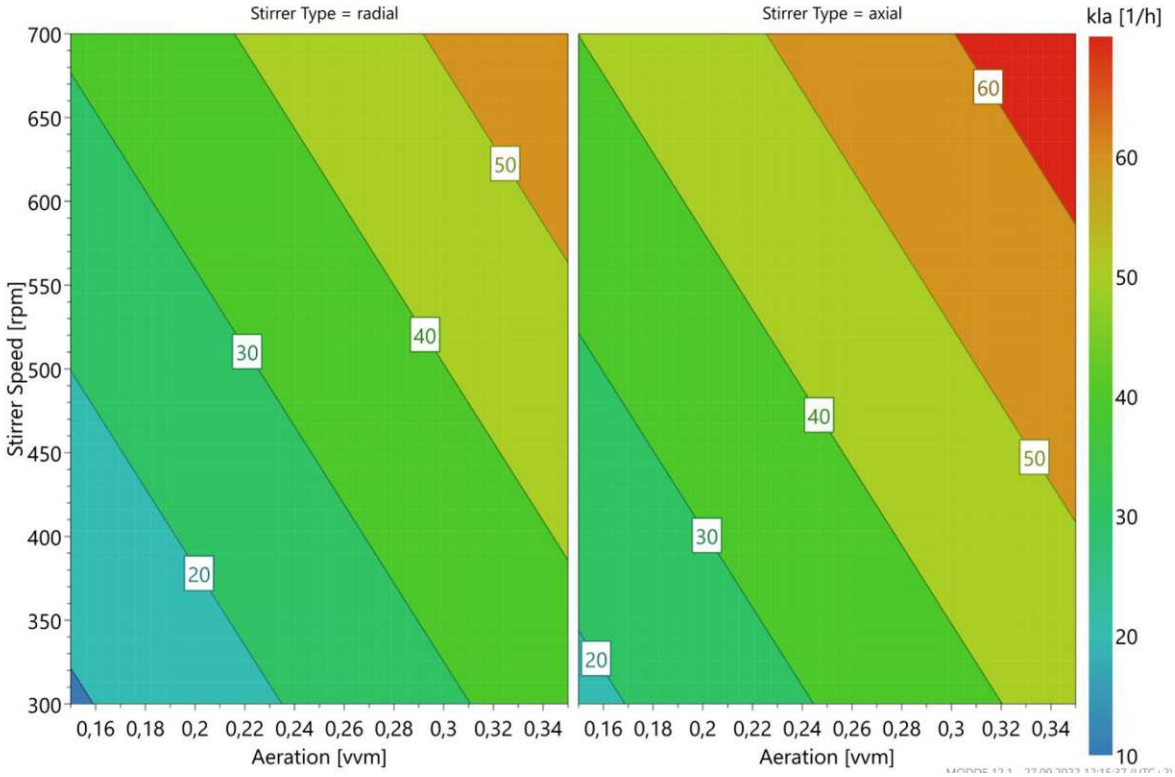

Figure 11: Contour plot of the model, predicting the increase of kLa with the descriptors stirrer speed, total gas flowrate and top stirrer type. Within the investigated design space, the correlations of kLa to the investigated variables seems to be linear. The axial top stirrer shifts the kLa higher across the entire design space. [model parameters: $R^2 = 0.888$; $Q^2 = 0.835$; $p_{Regression} < 0.01$; $F_{Regression} = 55.8$]

Next, the influence of the upper stirrer position relative to the surface was investigated. In this case the stirrer speed and air flowrates were set to the centre treatment of the DoE (500 rpm; 0.25 vvm), and two positions of the upper stirrer were compared: the “top position” where the impeller was very close to the surface, and the “mid position”, where the impeller was centred between the surface and the bottom stirrer (see Figure 6). In the top position, the axial stirrer

performed significantly better than the Rushton turbine, leading to the highest measured kLa of all upper stirrer configurations. However, in the mid position the Rushton turbine led to a slightly higher kLa than the axial stirrer. Therefore, the combination of a Rushton turbine in the mid position and the axial stirrer in the top position was tested as well. Interestingly, this led to worse oxygen mass transfer than either of the upper stirrers in their advantageous positions. We speculate this observation might be attributed to flooding of the impellers.

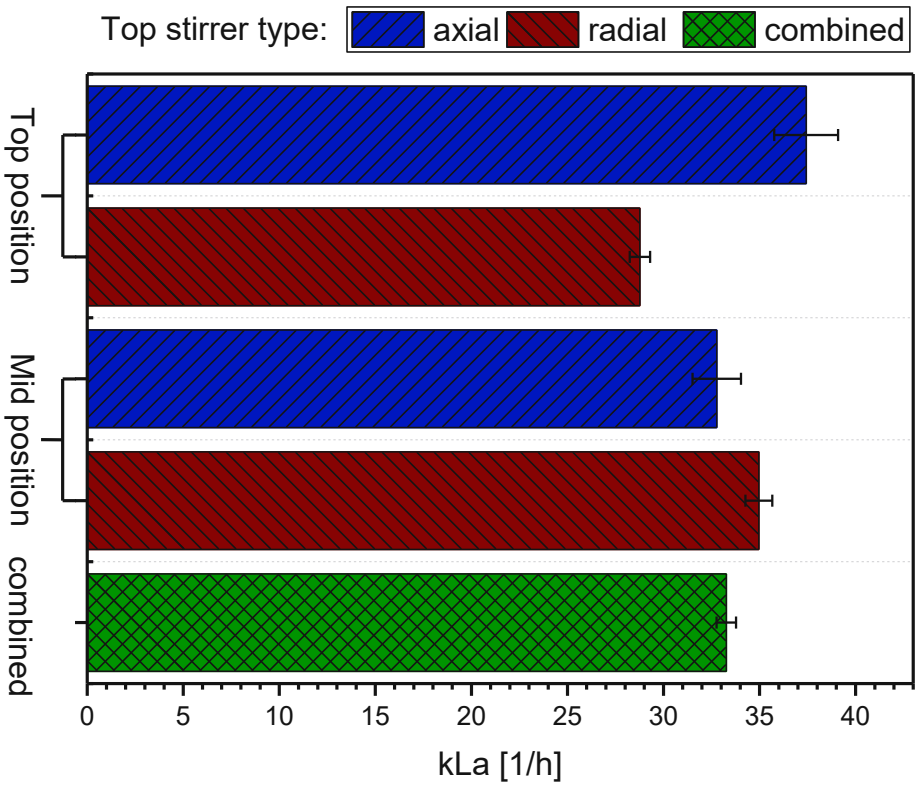

Figure 12: Comparison of the volumetric mass transfer coefficient resulting from different positional configurations and produced flow directions of the upper impeller.

Finally, the kLa improvement using the axial impeller was also tested at some common reactor conditions encountered within our working group that went beyond the limits of the investigated DoE. Firstly, we tested drastically higher agitation speeds and increased aeration conditions, at [700 rpm; 1.0 vvm] and [1500 rpm; 2 vvm] respectively. While still beneficial for the oxygen mass transfer, the difference between the impellers becomes insignificant when very high stirring and gassing rates are approached. We suspect this might be part of the reason why kLa optimization by means of the stirrer configuration can easily be overlooked: if the motivation is solely a very high oxygen demand, pushing agitation and aeration is still the most simple and effective way towards reaching that goal.

Finally, the impellers influence under the temperature of 75 °C, at which *S. acidocaldarius* is cultivated, was investigated as well. In this case, the axial upper impeller vastly outperformed the standard Rushton turbine by almost doubling the kLa. As gas solubility decreases with the temperature, higher mass transfer rates have to make up for a lower (c^*_{O2} - c_{O2}) gradient to keep up oxygen transfer. The increased gas holdup and mixing provided by a downward flow might contribute more to the mass transfer, than an increased exchange-area due to bubble dispersion under these conditions. This might make axial impellers particularly interesting for other thermophilic organisms.

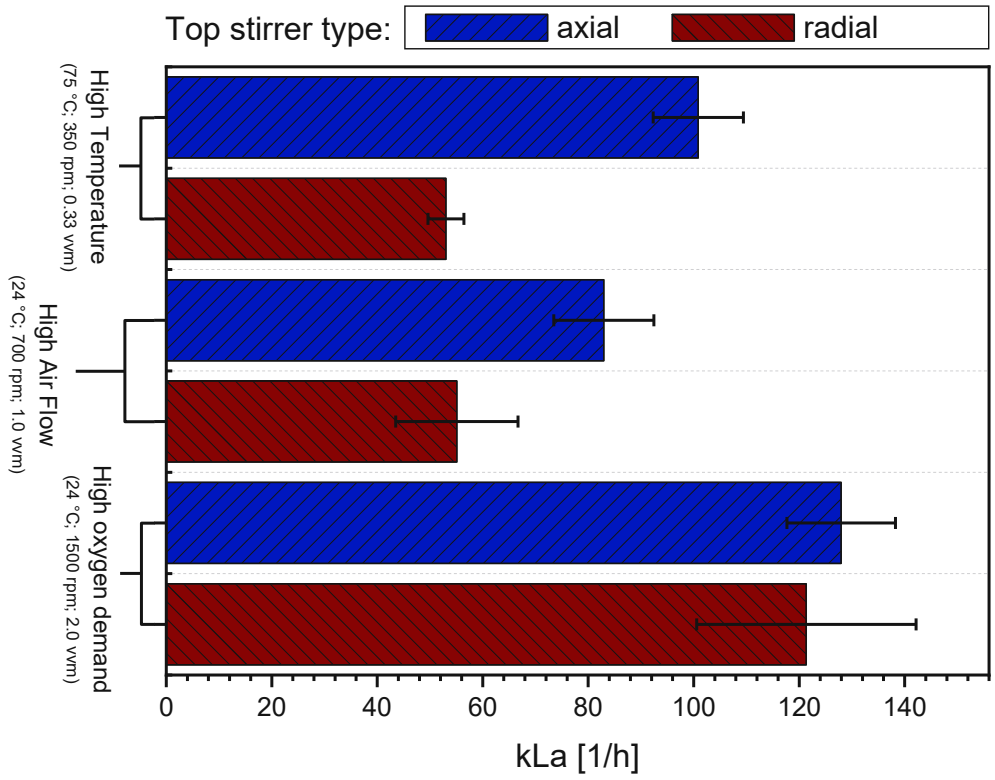

Figure 13: Results of testing the axial flow impeller in the "top position" close to the surface for conditions commonly used in our lab. The increase of the volumetric mass transfer coefficient when an axial impeller was used was especially prominent at high temperatures.

IV.4.3 Estimation of the power input

An estimation of the difference in specific power input between the two stirrer configurations is given in Table 1. The calculations were made for the standard fermentation conditions at which *S. acidocaldarius* is cultivated in our lab. The difference in estimated specific aerated power input amounts to 22 % less power drawn by the axial upper impeller compared to the conventional second Rushton turbine. Especially for a continuous cultivation that might run for

months without pause, this would be a significant cost reduction and might reduce wear on the motor of the stirrer.

Table 1: Estimation of the specific power inputs by using power numbers from the literature. The relative power demand under aerated conditions was estimated to be RPD = 0.9 for the Rushton blades, and RPD = 1 for the D3BS impeller based on the literature [62, 64]. Calculations were made for a stirrer speed of 350 rpm and aeration of 0.25 vvm.

Upper impeller	Specific unaerated power input $\frac{P_U}{V}$ [kW/m³]	Specific aerated power input $\frac{P_G}{V}$ [kW/m³]
2nd Rushton	0,41	0,37
D3BS	0,31	0,29

IV.5 Conclusions

The spatial constraints of small stirred tank fermenters, make mechanical foam control very difficult to achieve. Large rotary devices don't fit the standard lab-scale reactors, and ultrasound-based devices are not yet commercially available. However, the simple option of a foam breaker mounted to the main stirrer shaft couples the agitation intensity with the rotary speed of the foam breaker. This creates the problem of increasing primary foam stability along with the foam breakers efficiency. Additionally, the impeller within the headroom creates a highly stable secondary foam, that cannot be further compacted. Therefore, heavier foam loads likely cannot be controlled with this method. Multiple new foam breaker designs were tested, but the reduced bubble size after contact with the impellers led to increased foam build-up and prevented bubble coalescence. Ultimately, we concluded that foam mitigation is the more feasible approach in such situations.

Since oxygen demand is a key factor in aerobic fermentations, reducing the foaminess by decreasing agitation and gas flow must be compensated by increasing kLa using other means. Our results suggest that an alternative stirrer configuration can fulfil this requirement. The use of a downward pumping axial impeller instead of the typical second Rushton turbine in the upper submerged position significantly increased oxygen mass transfer, especially under lower agitation conditions. Notably, at 75 °C kLa was nearly doubled, which makes the proposed stirrer configuration very promising for the fermentation of thermophiles. A further benefit of the axial impeller is the decrease in power input, despite the increased mass transfer. If these results could be translated to larger scales, the proposed impeller arrangement would facilitate an environmental advantage as well.

IV.6 Appendix

IV.6.1 Notation

D … impeller diameter [m]

Fl_G … gas flow number [-]

Fr … Froude number [-]

g … gravitational pull [9.81 m/s^2]

N … impeller speed [1/s]

P_O … power number [-]

P_G … aerated power input [W]

P_U … unaerated power input [W]

Q_G … mean gas volumetric flowrate [m^3/s]

RPD… relative power demand [-]

V … liquid volume [m^3]

P_L … liquid density [kg/m^3]

IV.6.2 Flow regime map – Rushton turbine

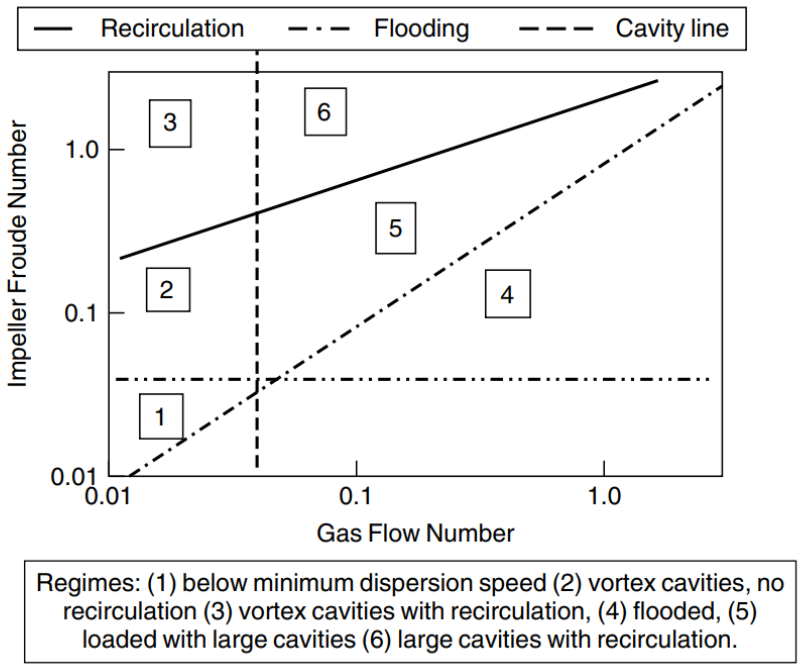

Figure 14: Flow regime map for a Rushton turbine with D/T = 0.4 as described by Paul et. al. [62]

V. Chapter B: In-line Cell Density monitoring for *Sulfolobus acidocaldarius*

V.1 Introduction

Typical foam-level sensors for bioreactors either use the conductivity of the liquid phase or dampening of an acoustic signal to detect foaming within a bioreactor. These often only provide a binary signal and are prone to fouling due to the remaining biomass after anti-foam addition is triggered. Another problem of conductivity-based sensors are false positives, due to media splashes, which can lead to catastrophic overfeeding of anti-foam. Novel approaches try to solve these problems by using imaging techniques [68]. However, even if the current limitations are overcome, monitoring foam levels to trigger the addition of anti-foam will always be confined to controlling a symptom instead of the cause. If the mitigation-based approach suggested in the previous chapter is to be implemented, it would be preferable to be able to predict foaming before it even occurs, and adapt the process accordingly.

The main surfactants within a bioprocess are proteins, lipids and the cells as particles themselves [10]. As the cell density within the fermentation broth is in direct relation to all of these factors, it stands to reason that measuring biomass could be used as a substitute, or at least as a basis for a soft-sensor, to monitor the surfactant concentration.

In the following chapter, three commercially available biomass sensors are tested on their ability to monitor the cell density of *S. acidocaldarius* under the extreme fermentation conditions this organism demands. Two of them are based on optical measurements: the Cell Growth Quantifier (CGQ; SBI) measures backscattered light at 521 or 940 nm wavelength, the Dencytee (Hamilton) measures optical density at wavelengths in the near infrared. The third probe, called Incyte (Hamilton), is based on dielectric spectroscopy. All three sensors are compared to off-line dry cell weight (DCW) and optical density measurements at 600 nm (OD_{600}) as the “gold standard”.

V.2 Methods and Materials

V.2.1 Foam levels at different protein concentrations

Within a 2 L glass fermenter, foam was generated by sparging compressed air through 1.6 L of a skimmed milk protein (SMP) solution of various concentrations between 5 g/L and 20 g/l. The foam height was measured after remaining constant for 3 minutes. If foam reached the top

of the reactor (100 mm) the experiment was ended. The medium was generated by first mixing the protein powder to a paste with small amounts of deionised water, and then adding more water until the final volume was reached while mixing with a metal spatula.

V.2.2 Fermentation set-up

The continuous cultivations of the strain Sulfolobus acidocaldarius DSM 639, obtained at German Collection of Microorganisms and Cell Cultures (DSMZ, Germany), were grown within a 2 L glass fermenter (Biostat A-plus, Sartorius, Germany). The cells were cultivated on Vienna Defined (VD) medium [47] using L-mono-sodium glutamate (MSG) and D-glucose as C-sources. For better readability the biomass concentration is given as "normalized cell density" (ncd) with a value between 0 - 1 ncd, with 1 ncd referencing the final production cell density. This final production biomass concentration was confirmed during a reproducibility study and shown to be a reliable reference for this process. Normalization was performed, by dividing the measured cell density (OD_{600} or DCW) through this standard production cell density.

A constant volume during the chemostat phases was kept by continuously pumping out reactor bleed, through a bleed valve. Throughout the whole process, stirring was kept at 350 rpm and temperature was controlled at 75 °C with a rubber heating mantle. The pH of 2.7 was controlled using an Easyferm Plus Electrode (Hamilton, USA) for monitoring and automatic addition of 4.8 % (v/v) H_2SO_4. Pressurized air was sparged through a sintered steel microsparger at a constant rate of 0.25 vvm. The CO_2 concentration within the off-gas was measured using a BCP-CO_2 (Bluesense, Switzerland) off-gas analyser.

V.2.3 In-line sensor signals

The two probes by Hamilton (Incyte Dencytee) were installed into the bioreactor through a standard 13.5 Pg slot. The signal was recorded using an Arc View 265 Transmitter (Hamilton). The CGQs sensor Plate was fixed to the glass wall of the reactor within the open space between the ends of the rubber heating mantle as is shown in Figure 15. It was connected to a laptop where data acquisition and calibration were performed using the CGQs proprietary software.

Figure 15: The CGQs sensor head fixed to the glass wall of a 2 L glass fermenter.

V.2.4 Calibration of the CGQ sensor

To get the best results, an extensive calibration procedure for the CGQ sensor had to be performed: First a set of concentrated stock solutions were created, by centrifuging fermentation broth and resuspending the pellets with various amounts of supernatant. Three solutions were prepared this way: 1 L with OD_{600} 2; 1.5 L with OD_{600} 18.6; 1 L with OD_{600} 48. A 12-point calibration was created by successively removing defined volumes from the reactor and replacing them with stock solutions at a total working volume of 2 L. The resulting cell suspensions within the reactor were sampled and OD_{600} was determined in triplicates. Finally, the backscatter measurements of the sensor were correlated to the off-line OD_{600} data. (Stirrer speed, aeration, temperature etc. are all process parameters included within the full sensor calibration).

V.2.5 Off-line biomass measurements

For the off-line biomass measurements about 10 mL samples were taken out of the reactor and immediately cooled down to room temperature in a water bath.

From this sample, dry cell weight (DCW) was measured in triplicates by centrifuging 1960 µL sample in tared 2 mL Eppendorf tubes for 10 minutes at 20,000 rcf and 4 °C. After

discarding the supernatant, the samples were dried at 120 °C over three days before being weighed.

The optical density at 600 nm (OD_{600}) was measured against a blank of purified water with an ONDA V-10 PLUS spectrometer (XS instruments, Italy).

V.2.6 Off-line dielectric spectroscopy experiments

Some preliminary experiments and the off-line permittivity measurements mentioned in this work were conducted using two FOGALE Biomass System sensors. Hamilton assured us that the basic technology was equal to the Incyte sensor, as the sensor technology was bought and further developed by under the new name.

For the measurements, fresh samples were taken from a continuous *S. acidocaldarius* culture and immediately used for the experiments. The samples were kept at 75 °C in a tempered water bath and shaken before measurements to minimize sedimentation. To investigate spatial limitations interfering with the electric field, sensor usage within a 15 mL falcon, a 50 mL falcon, and a 100 ml Schott bottle was tested. Temperature influence was investigated after cooling down samples to room temperature under running tap water. Finally, to test the sensor-integrity, samples of an *Escherichia coli* DE3 fermentation with OD 3.6 and pH 8 were measured at 36 °C using different dilutions.

V.2.7 Electric Impedance Spectroscopy

A fresh 100 ml sample of a continuous *S. acidocaldarius* fermentation was aliquoted and centrifuged for 10 minutes at 24 °C and 3000 rcf. After pooling the supernatants, the remaining pellets were resuspended with different amounts of supernatant, to receive solutions of different biomass concentrations (0 g/L; 2.3 g/L; 3.5 g/L; 7.0 g/L). The resuspended biomass solutions were immediately reheated to 75 °C within a tempered water bath, upon which electric impedance spectroscopy measurements began.

The measurements were conducted using a Novocontrol NEISYS Electrochemical Impedance System, at 10 mV amplitude, 0 V Bias, and triplicate measurements (after 0 s, 120 s, 240 s). Scanned AC Frequencies ranged from 10^6 Hz to 0.135 Hz, separated into 48 data points. An in-house built probe, consisting of two round, austenitic, stainless steel electrodes with a diameter of 10 mm positioned with a 2 mm gap in between [69] was used. The probe is depicted in Figure 16.

Figure 16: In-house built EIS probe, using stainless steel electrodes.

V.3 Results and Discussion

V.3.1 Cell Density as determining factor for foam build-up

The effect of surfactant concentration on foaminess was investigated by measuring the constant foam level produced by agitation and air sparging of different skimmed milk protein (SMP) concentrations. The averages of measurements done in duplicates are shown in Figure 17. At 5 g/L SMP foam levels remained within a small range, but a slight increase with agitation and gas flowrates could still be seen. When 15 g/L SMP were used, foam levels varied from 30 mm to complete overflow (= 100 mm). Since this was observable within a rather small range of agitation/aeration conditions, this medium was used as an approximation for fermentation broth at the surfactant concentration where the process starts to overflow. When the protein concentration was raised to 20 g/L SMP, even the lowest stirrer speeds and gassing rates led to overflow. While these results display the massive influence that agitation can have on the formation of foam, they also show that the surfactant concentration determines if this influence even matters. At sufficiently high concentrations any meaningful amount of gassing or agitation will lead to an overflowing reactor. Therefore, attempting to predict the foaminess of a process must involve the monitoring of surfactant concentrations. When the product is the biomass itself, or the product directly correlates to cell growth, surfactant concentration should be mainly correlated to the biomass concentration. If the product formation is not directly linked

to the cell growth, the product concentration would likely need to be monitored as well. As biotechnological products are usually proteins, they could strongly affect media foaminess.

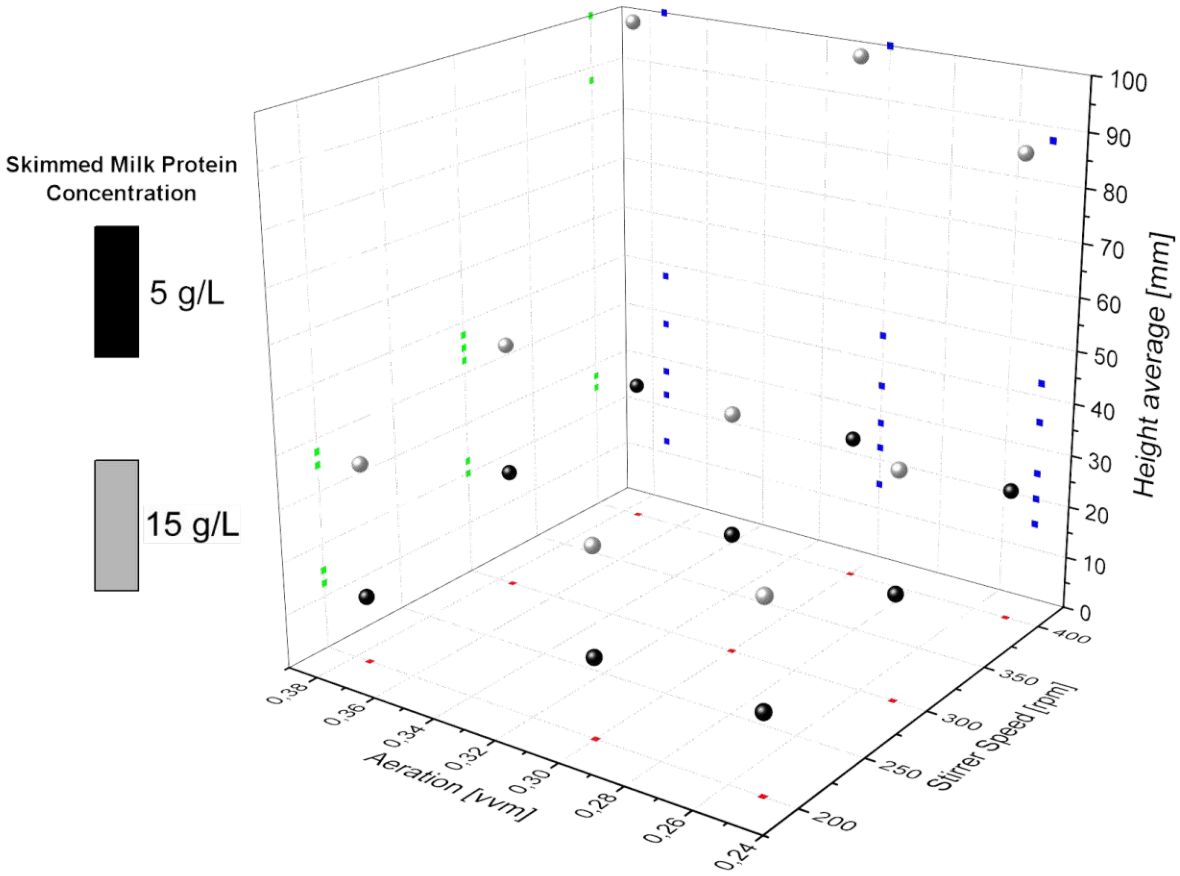

Figure 17: Measured Equilibrium Foam heights at different stirrer speeds and aeration levels. Black points were measured using 5 g/L skimmed milk protein as foamy medium. Grey points used 15 g/L SMP as foamy medium. Since 100 mm was the distance between liquid surface and headplate, a height of 100 mm within the diagram represents the fermenter overflowing.

V.3.2 Dielectric spectroscopy

V.3.2.1 Hamilton Incyte Sensor

The Incyte sensor uses dielectric spectroscopy to measure the permittivity of the fermentation medium, which then can be correlated to the cell density. It is built in a standard reactor probe format, only requiring about 1 cm of free space around the electrodes located at the probe head. Surrounding these electrodes an electric field is generated, in which the permittivity is measured. Figure 18 shows a first test run including the Incyte sensor.

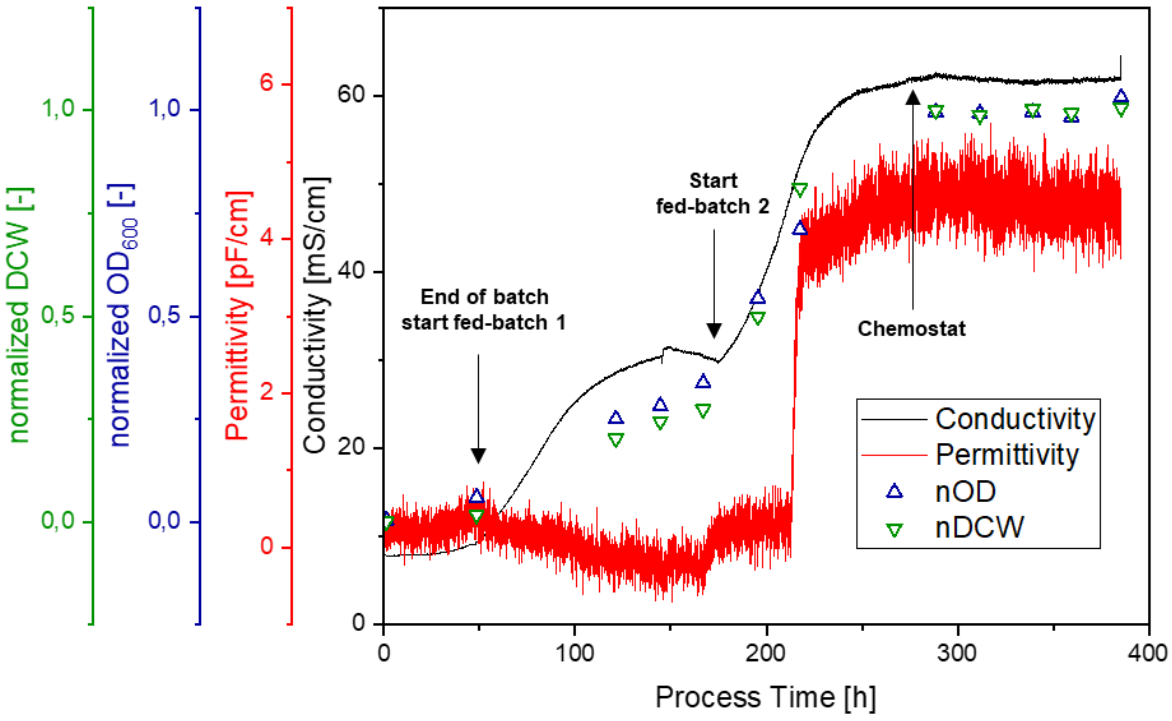

Figure 18: first test run of the Incyte cell density sensor. The permittivity does not fit the normalized cell density data measured off-line. The conductivity that is also measured by the probe nicely shows the progress of the individual progress steps

The measured permittivity did not fit the cell density throughout the process, first decreasing until the final fed-batch phase, and then suddenly drastically increasing towards the continuous fermentation phase. In general, the signal was very noisy. However, the included measurement of the media conductivity was an unexpected benefit, as it provided a good indication of the current process phase. For example, it was easy to see when the chemostat phase had reached its steady state. An observation that was more difficult based on cell density measurements alone.

The probe also allows to record the individual permittivities measured at specific AC frequencies - the final permittivity attributed to the cells is calculated from the difference between a high frequency and a low frequency. This is done, so that background influences on the lower frequencies can be corrected by the less sensitive high frequencies. An overview of the measured frequencies is shown in Figure 19. As it is to be expected, the lower the AC frequency was, the more change in the signal could be observed. Even at the lowest measuring frequency the probe allowed (300 kHz), very little signal was observed. However, an interesting observation was made between 50 h and 100 h process time, which corresponds to the first fed-batch phase. A small decrease of the signal to a negative permittivity, before an increase towards 0 pF/cm again. Disregarding the physical impossibility of a truly negative permittivity, the

relative trend is also surprising. In theory the permittivity should increase with the growth of cells. This oddity of measuring negative permittivity was also observed during off-line experiments detailed later, but no definitive explanation was found. In an attempt to increase relative differences in the signal for future experiments, the frequency pair that was used for the permittivity measurements was adapted to 500 kHz lower plateau frequency and 10000 kHz upper plateau frequency.

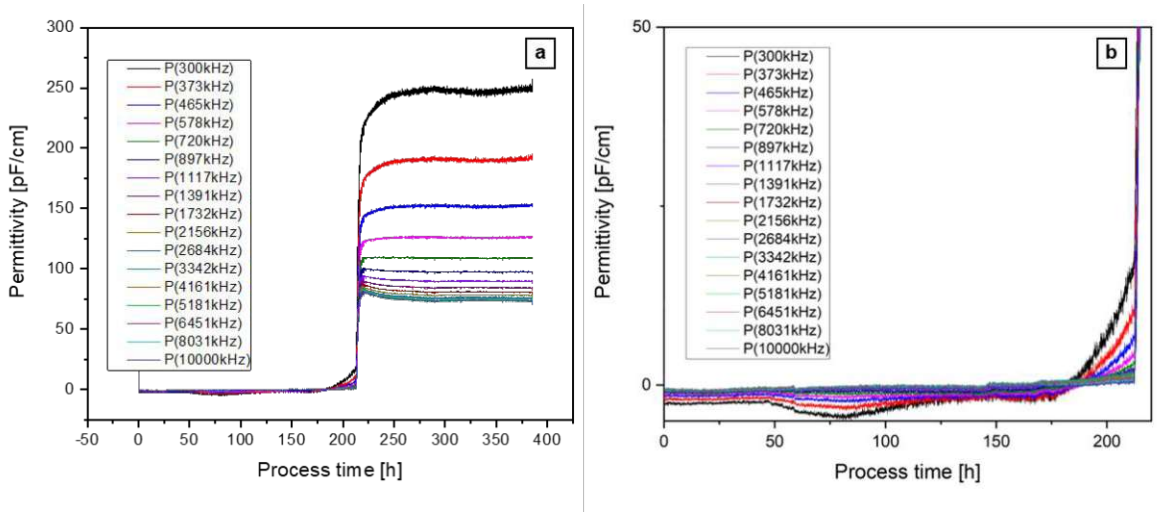

Figure 19: Permittivities of the individual frequencies measure during the fermentation shown in Figure 18 for the whole process (a) and a zoomed in time selection (b). At the lower frequencies the permittivity can be seen slightly decreasing during the first fed-batch phase (between 50 h and 100 h process time).

V.3.2.2 Lowering the conductivity

The conductivity of the fermentation medium generally was quite high, exceeding the probes maximum specifications of 50 mS/cm in later process stages. By adjusting the feed concentration, the conductivity was lowered and raised above 50 mS/cm during a running continuous fermentation. It can be clearly seen in Figure 20 that the jump in permittivity coincides with going above the probe´s conductivity specifications.

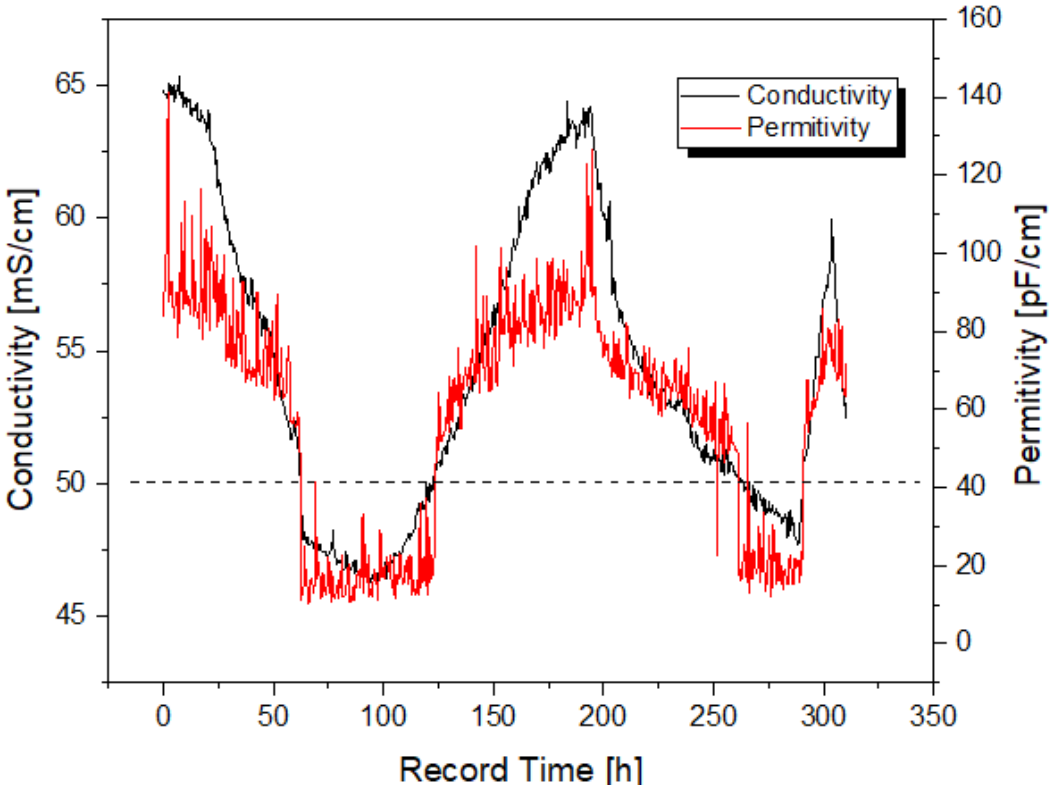

Figure 20: Experiment with Varied feed concentration during chemostat, to repeatedly lower and raise the conductivity below and above 50 mS/cm (indicated by the dotted line). The permittivity clearly "jumps" at this threshold.

Aiming to possibly improve upon the permittivity data, another run with a reduced $(NH_4)_2SO_4$ concentration of the medium was attempted. The measured conductivity and permittivity during this fermentation are plotted against off-line cell density data in Figure 21. From the beginning until the point indicated at about 250 h process time, 40 % of the $(NH_4)_2SO_4$ concentration compared to a standard run were used. After this point it was once more lowered to 30 %. Despite decreasing the conductivity relative to the cell density within the reactor, the permittivity signal remained very noisy. Changing the lower measuring frequency led to higher relative permittivity shifts. However, any trend fitting the off-line cell density can only be observed at normalized cell densities of 0.3 ncd or higher. Due to problems with contaminations, the experiment had to be cancelled before higher cell densities could be reached. However, because there was no sign of improving the poor signal quality, and time reasons, the experiment was not repeated.

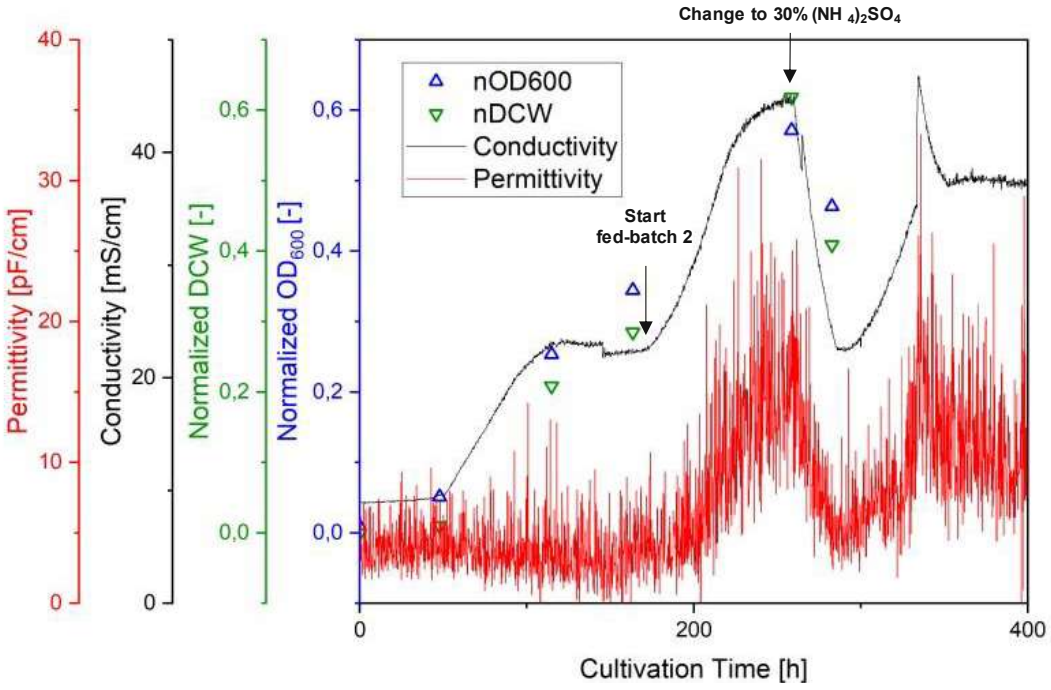

Figure 21: Incyte sensor data for a fermentation attempting to stay below 50 mS/cm media conductivity by reducing the $(NH_4)_2SO_4$ concentration. The adapted measuring frequencies lead to higher observed permittivity, yet signal quality remained poor.

V.3.2.3 Off-line Experiments

Some further off-line experiments were conducted to investigate possible influence factors that seem to prevent successful permittivity measurements for *S. acidocaldarius*. A graphical summary of the results is given in Figure 22. For availability reasons, two older probes using the same technology as the Incyte probe were used. Generally, even lower (negative) permittivity values were measured with these older sensors.

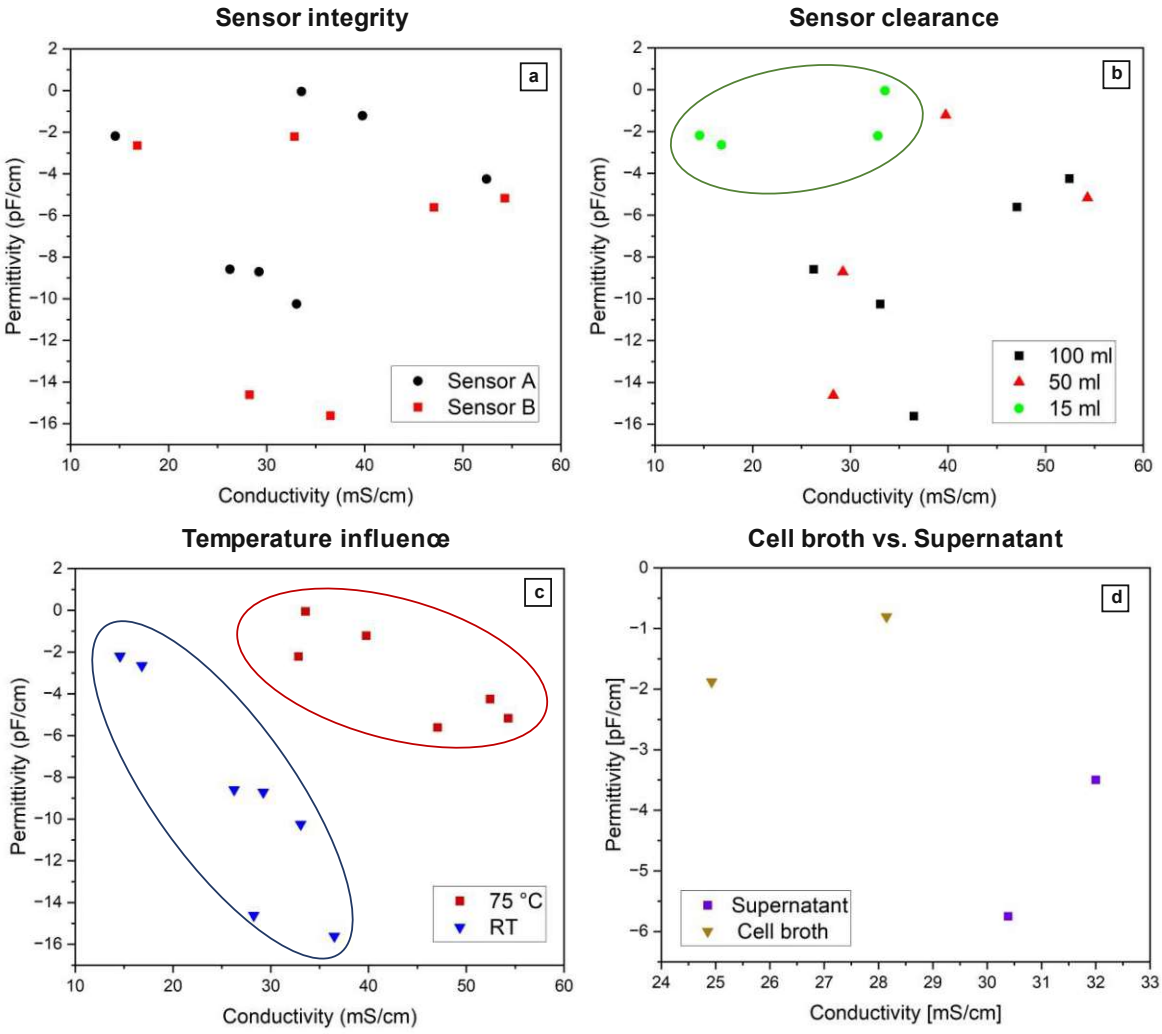

Figure 22: Off-line tests to check for potential problem factors. Two identical probes (a), probe clearance to the vessel walls (b) by measuring in differently sized vessels, as well as temperature influence (c) were investigated. Afterwards cell suspension was compared to cell free supernatant at room temperature (d).

Two identical sensors using the same technology were compared, to check for deviations between individual sensors. While one of the probes generally seemed to measure lower permittivities, the observed trends were the same. As a calibration would be necessary to measure cell density anyways, slight deviations between individual probes would be inconsequential.

Different spatial conditions were tested via adaptation of the vessel size in which the measurements were conducted. The measurements within 15 mL falcons led to a significantly lower difference in signal for otherwise differing conditions. Here the clearance of only a few millimetres between electrodes and walls is apparently too small for the electric field to be properly established. Compared to the 100 mL Schott bottle, in which the recommended minimum distance of 1 cm was easily given in all directions, measurements in 50 mL falcons seemed to be largely the same. However, one measuring point did seem to cluster with the 15 ml

falcon points. Also, during the experiment with *Escherichia coli* described further below, two outliers were observed when measuring within a 50 mL falcon. This suggests that it is principally possible to adequately space the probe within a 50 mL falcon, but the leeway for errors is small. If the electric field is hindered, less signal is observed. However, within the fermenter used for our experiments, about twice the circumference given within a 50 ml falcon is free from other parts around the probe. Therefore, spatial limitation is very unlikely to be the issue behind the poor performance.

The increase in temperature seems to coincide with a higher conductivity, which is in line with expectations of the conductive behaviour of liquids. The measured permittivity also was also higher at 75 °C compared to room temperature. Since this too matches the expected trend from the literature [70], there is no reason to assume that the temperature might be the reason for the low, or respectively negative permittivity measured for *S. acidocaldarius.*

Finally, the fermentation broth was compared with cell free supernatant. Since a higher permittivity was observed for the samples which contained cells, one can conclude that *S. acidocaldarius* cells do have an influence on the permittivity. This might point to the used media itself being the reason for the low signal. A possible next step could have been to wash cells and resuspend them in a standard buffer, like phosphate buffered saline, and see if a positive permittivity value would result. If that was the case, one could measure the permittivity of solutions containing the individual buffer components, to find out if a specific compound causes the issues.

The functional integrity of the probes used for the off-line measurements was also tested by measuring a sample of an *E. coli* DE3 fermentation with OD 3.6 in different dilutions. As mentioned above, the clearance around the probe was also investigated again during this experiment. The resulting data is given below in

Table 2. For *E. coli* low but positive values for the permittivity could be measured, and besides some above discussed outliers, the dilutions were depicted fairly accurate within the measurements.

In summary, while the off-line experiments gave no conclusive explanation as to why dielectric spectroscopy probes do not seem to work for *S. acidocaldarius*, they did highlight the unexpected behaviour of measuring negative, and thus physically senseless, permittivities.

Table 2: Off-line permittivity measurement of E. coli to verify the probes functionality.

Experimental Order	Vessel type	Dilution factor	Measured data		Dilution corrected	
			Conductivity (mS/cm)	Permittivity (pF/cm)	Conductivity (mS/cm)	Permittivity (pF/cm)
1	100 ml	1	27,47	1,48	27,47	1,48
2	50 ml	1	25,68	1,04	25,68	1,04
3	100 ml	1	26,11	1,14	26,11	1,14
4	100 ml	2	14,73	0,58	29,45	1,16
5	50 ml	2	14,41	0,37	28,83	0,75
6	100 ml	4	7,66	0,24	30,64	0,96
7	50 ml	4	7,11	0,03	28,45	0,11
8	50 ml	2	13,09	0,48	26,18	0,96

V.3.2.4 Electric Impedance Spectroscopy

As the in-line data of the Incyte showed more response at lower frequencies, but the probe itself only allows measuring frequencies upwards of 300 kHz, electric impedance spectra (EIS) of live cells at different cell concentrations were measured. The resulting Nyquist plots are depicted in Figure 23. As expected, larger differences between different cell concentrations were observed at lower AC frequencies. However, the shifting of the curves towards lower real parts of the impedance with rising biomass concentration was a very interesting result. Previous measurements by Slouka et. al. [71] showed the inverse trend for *E. coli* samples. As the x-axis corresponds to the real part of the impedance, this strange dielectric behaviour by *S. acidocaldarius* might be related to the negative permittivities that were measured.

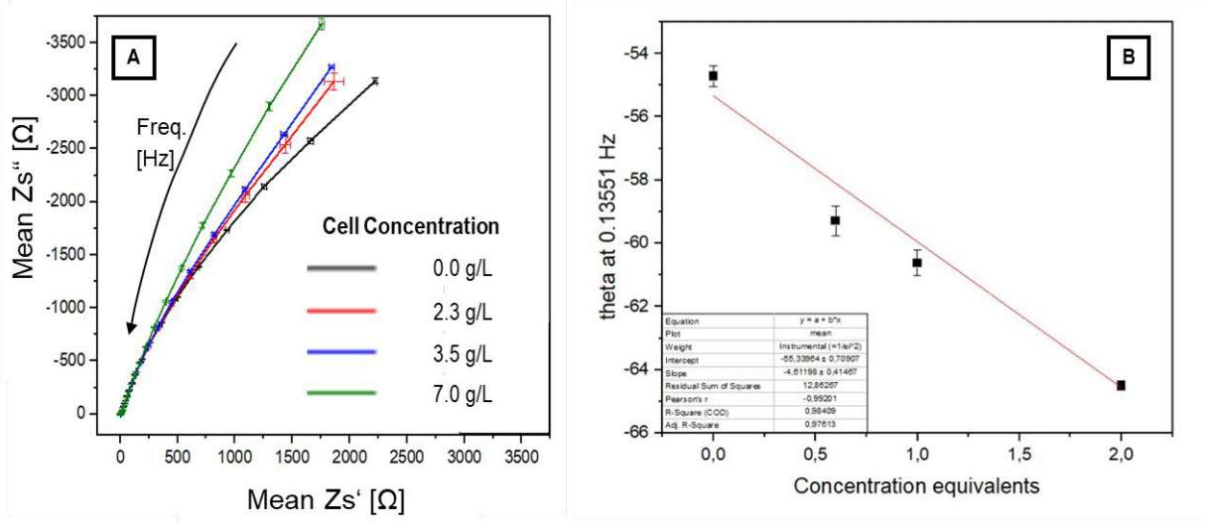

Figure 23: A) Nyquist plots of Sulfolobus acidocaldarius fermentation broth at different cell concentrations. Alternating current frequency is increasing towards the bottom left of the plot. The observable effect of the cells on the proportion of real and complex shares of the impedance is exceedingly higher at lower current frequencies. B) Correlation of the currents gyration (theta) at 0.13551 Hz and cell concentration. The observed correlation shows that in principle, using the cells influence on the electric field to measure cell density should be possible.

Using the measured results, a linear correlation between the gyration of alternating current at 0.13551 Hz and the biomass concentration could be observed (Figure 23/B). Theoretically, this correlation might be usable to measure biomass in-line using EIS.

However, according to the manufacturer, the reason for the Incyte's minimum measuring frequency of 300 kHz is that the noise caused by other media components at such low frequencies often makes reliable measurements impossible. While a measuring method could possibly be developed for very specific conditions, it would likely not be very robust against media variations and therefore not transferable to other processes. Hence, *S. acidocaldarius* might not be a suitable organism to have its cell density measured by analysing its dielectric properties.

V.3.2.5 Conclusion

While dielectric spectroscopy seems to be a successful method to measure the cell density of a variety of microorganisms including procaryotic bacteria, eucaryotic yeast, algae, and even tissue cells [69, 72, 73], it does not seem to work easily for *S. acidocaldarius*. Our experiences with probes based on the method were dominated by poor signal quality and non-explicable negative permittivity measurements. When measuring EIS spectra, the observed trend of the Nyquist plot with changing biomass concentrations was inverse compared to data for *E. coli.* As there seems to be no published literature on dielectric spectroscopy being used to determine archaeal biomass concentrations, it might be possible that some electrochemical attribute of archaeal cells might prevent this method from being applicable.

V.3.3 Cell Growth Quantifier (CGQ)

V.3.3.1 First impressions

The Cell Growth Quantifier (CGQ) by SBI measures cell density by pulsing light from LEDs into the fermentation broth, which is then backscattered by the biomass and detected with a photodiode. Since a higher cell concentration will lead to more backscattered light, a correlation between the backscatter and cell density can be made. During the fermentation depicted in Figure 24, the CGQ sensor was installed during an active continuous *S. acidocaldarius* fermentation.

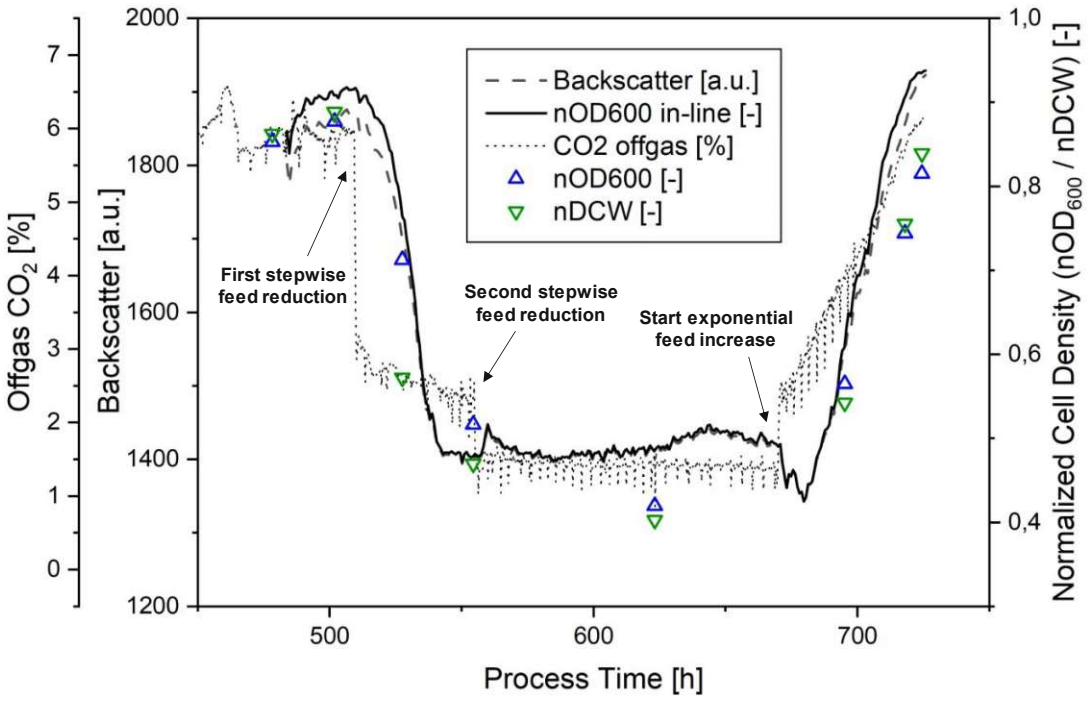

Figure 24: First test of the CGQ by attaching it during a running fermentation. Differences in cell density were induced by two stepwise reductions of the feed concentration, and a final exponential increase in feed concentration. Besides the raw backscatter signal and cell density data, the CO_2 concentration in the off-gas was also plotted, as they clarify the timings of the feed alterations.

The default calibration from the software was used, and continuously improved by including off-line OD_{600} data immediately after it was measured. The general trend of the off-line cell density was depicted quite well, but the drop within the cell density from about 550 h to 675 h process time was not reflected within the backscatter signal. No definitive reason for this behaviour could be found, but as foaming is cited as a common problem for the CQG by the manufacturer, this might be one of the reasons for this unexpected behaviour.

V.3.3.2 A full standard fermentation

After the extensive calibration of the CGQ for our specific process was performed according to the protocol detailed within the software (see V.2.4 Calibration of the CGQ sensor), a full fermentation including the CGQ from the start was carried out. In addition to the calibration, all off-line OD_{600} measurements during the reactor run were used to continually update the calibration. The resulting backscatter and in-line OD_{600} signals are compared to the off-line OD_{600} and cell density measurements in Figure 25.

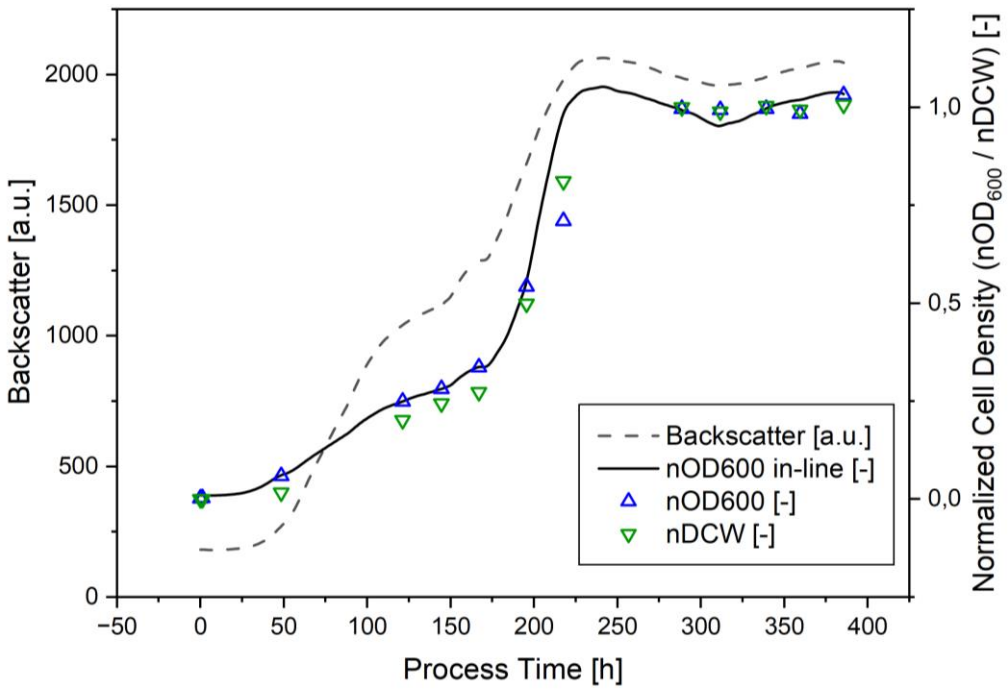

Figure 25: Full standard fermentation run using the CGQ to measure cell density in-line. The raw backscatter signal as well as the OD_{600} resulting from the final updated calibration are plotted against the off-line biomass data.

The in-line OD_{600} data resulting from the fully calibrated sensor matched the off-line data very well, with the only exception being a short phase during the final fed-batch phase at around 200 – 250 h process time. Since the off-line DCW and OD_{600} correlate very well, the measuring error is likely to be either coming from the backscatter signal, or resulting from a sampling error (as OD and DCW were measured from the same sample). As the CGQ combines three different functions to calibrate the backscatter signal to the off-line cell density (first exponential, then sigmoid, finally linear), the error might be due to a simultaneous steep increase in cell density at the same time the calibration-function switched.

Another important observation was, that the backscatter fit the optical density less well when no off-line data point was available for the current cell density. This is due to the fact, that there will always be small inconsistencies between the different reactor runs such as scratches in the glass, the exact position of the probe-head, and inconsistent angles and positions of reflective metal parts inside the fermenter. Therefore, supplementary off-line data will always be required to fine tune the CGQs calibration for an individual run.

V.3.3.3 Conclusion for the CGQ

In summary, I would describe the CGQ as a very promising analytical tool, to close the information gap between samples after a run is finished. The nonintrusive nature of the sensor allows to collect this supplementary data without risking influencing the process or requiring

an additional probe port, which can be a limiting for bench scale reactors. However, the requirement for off-line calibration-data each run to achieve precise measurements limit the CGQ in its potential to actively monitor and control the cell density. A further limitation in this context, is that at the time of writing this thesis no data signal interface such as 4 – 20 mA output are available. Therefore, the CGQs signal cannot be integrated into any process control system, and is limited to the proprietary software platform of the manufacturer.

V.3.4 Hamilton Dencytee

The Hamilton Dencytee probe measures the media turbidity within the near infrared (NIR) spectrum, which correlates to the cell density. It operates directly within the reactor connected through standard 13.5 Pg probe port and can be connected to a process control system via 4 – 20 mA data signal interface. In Figure 26 the in-line measured absorbance is plotted against the off-line measured DCW and OD_{600}. Overall, the Dencytee's data fit the off-line measurements very well, linearly correlating with OD_{600} with a correlation coefficient $R^2 = 0.942$.

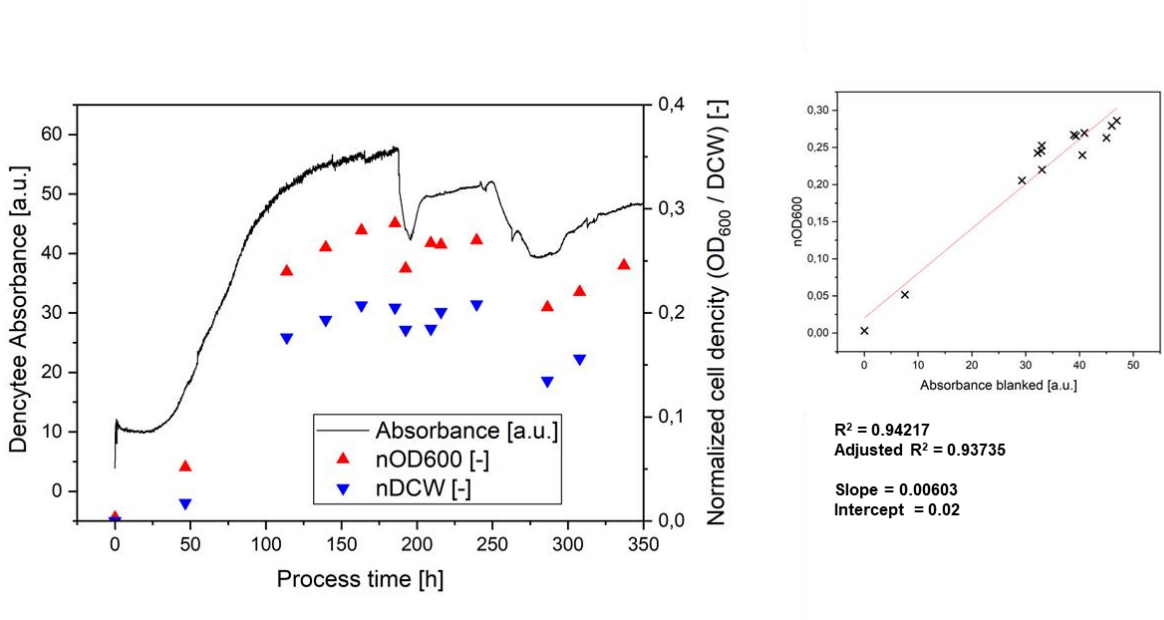

Figure 26: NIR-Absorbance measured in-line by the Hamilton Dencytee probe, plotted against off-line cell density data. Due to difficulties with the fermentation, only lower cell densities compared to a standard run were achieved. A linear correlation between absorption units and off-line OD_{600} is shown on the right side.

The received signals quality looks very good, and no physical damage to the probe caused by the high temperature and acidic environment of the fermentation was observed. A rather high deviation of the off-line measured DCW and OD_{600} normalized biomass concentrations has to be noted. Since the optical density is more sensitive at very low cell densities, but dry

cell weight more robust at high concentrations, normalization of both metrics by division through a maximum standard concentration led to the normalized DCW undervaluing the cell density at low concentrations. Due to problems with the fermentation, only these lower biomass concentrations were reached. This limited the recorded data to about a third of the usual cell density range of the process.

Nonetheless, the correlation of the absorption signal to the normalized OD_{600} was chosen to create a crude calibration function. This allowed calculating an in-line OD_{600} for the fermentation, which is plotted against the corresponding off-line OD_{600} as shown in Figure 27.

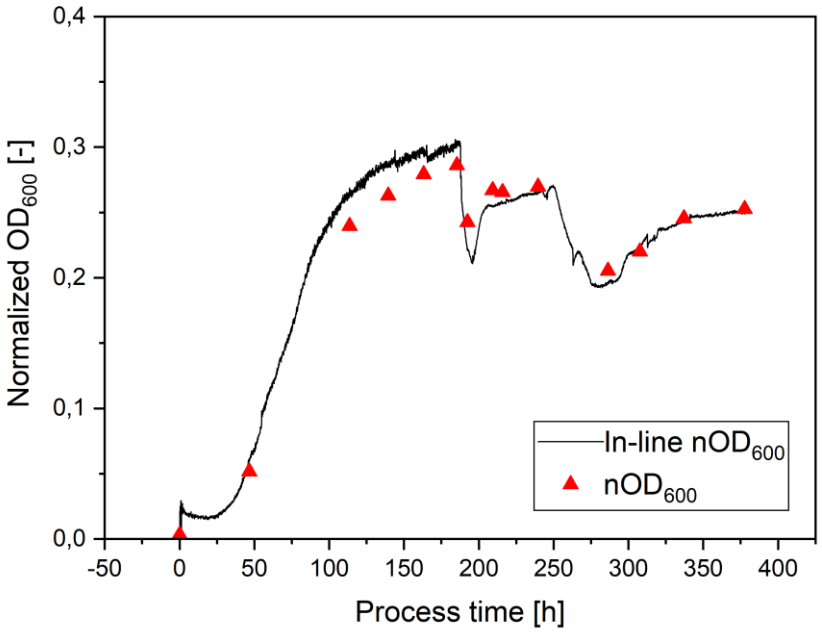

Figure 27: In-line OD_{600} calculated from the absorption signal using the correlation shown in Figure 26.

While these first impressions seem very promising, more experimental evidence would be needed. The next steps would be to create a calibration function across the entire biomass concentration spectrum of the process from one fermentation, and then try to monitor the in-line cell density of another fermentation. This would show that the probe provides reproducible data that allows real-time cell biomass measurements, without the need to recalibrate with off-line data from the same run. Also, it would be ideal if the linear range of the correlation between NIR-absorption and biomass concentration exceeded the maximum expected cell density of the process. The possibility of integrating the sensor via 4 – 20 mA signal interface into any process control system combined with the high signal quality would make this sensor a highly promising PAT tool for *S. acidocaldarius*, if these requirements were fulfilled.

VI. Conclusion

VI.1 Scientific questions

i. How does a headspace impeller affect excessive foam build-up in a laboratory-scale bioreactor?

The spatial limitations of lab-scale bioreactors make the control of intense foaming via mechanical means all but impossible. Highly efficient mechanical foam-breaking systems require additional space and sterile couplings, as well as separation of the secondary foam, both of which are normally not available at this scale. Mounting a simple foam breaker to the main stirrer shaft couples the already limited efficiency of such a device with increased primary foam stability due to agitation. The added stability of the secondary foam produced by a headspace impeller can lead to even more foam build-up than an empty headspace, where drainage and bubble coalescence are not hindered. Therefore, increasing the efficiency of a foam breaker mounted to the main stirrer shaft seems pointless past a certain foaminess of the medium.

ii. How does a downward pumping axial stirrer close to the surface affect the volumetric mass transfer?

As main factors of foam generation, the reduction of agitation and aeration can significantly reduce foam build-up. Therefore, lowering these parameters to the minimum necessary to meet oxygen demand could be a viable approach for foam control in small scale fermenters, when chemical anti-foams are not wanted, and mechanical control is impossible. To enable this reduction, alternative methods of increasing volumetric mass transfer between the gaseous and liquid phase are demanded. The results obtained during this thesis show, that using a downward pumping axial stirrer instead of the typical second Rushton turbine as upper impeller can increase kLa values, especially for low agitation conditions. Besides aiding foam control, increasing the mass transfer in this way also might provide environmental advantages at larger scales, due to reduced energy consumption. These results may also be relevant for processes with high oxygen demand but limited agitation possibilities, such as with shear sensitive cells. Furthermore, the increase in kLa was especially pronounced at 75 °C, making the stirrer configuration attractive for *Sulfolobus acidocaldarius* and other thermophiles.

iii. How is the performance of three commercially available in-line biomass sensors affected by harsh conditions like high temperature and low pH?

The examined sensors that use optical methods (Dencytee, Hamilton; Cell Growth Quantifier CGQ, SBI) both worked well, despite the challenging conditions. Neither the high temperature of 75 °C nor a constant pH of 2.7 seemed to harm the probes, and the obtained signals retained good quality for long durations of up to 400 h.

Although this feature is planned, at the time of writing the CGQ cannot be connected with third party process control systems but is limited to the DOTS platform of SBI. Another disadvantage is the need to continually refine the sensors calibration with off-line data for each fermentation. However, as a data analysis tool to close the information gap between off-line measurements, the CGQ performed very well.

Due to the accessibility of the standard 4 – 20 mA signal interface, the Dencytee sensor seems very promising as monitoring tool for *S. acidocaldarius*. If future experiments can show that it performs just as well at higher cell densities, and no extra calibration between individual runs of the same process are necessary, it could be used to experiment with biomass control strategies.

The experiments with the Incyte (Hamilton) sensor did not give promising results. Despite the efforts to improve upon the poor signal quality, no definitive explanation for the high noise and negative permittivity data could be found. However, during electric impedance spectroscopy measurements of *S. acidocaldarius* samples, a clear effect of the cells on the impedance was observed. With increased cell density, the curve within the Nyquist plot was shifted towards smaller real parts of the impedance. An observation contrary to the behaviour that cells like *E. coli* show. This strange electrochemical characteristic of *S. acidocaldarius* might be an interesting topic for future research.

VII. Appendix

VII.1 References

[1] A. M. Buswell and S. I. Strickhouser, 'Some Observations on Sewage Tank Gases', *Ind. Eng. Chem.*, vol. 18, no. 4, pp. 407–409, Apr. 1926, doi: 10.1021/ie50196a022.

[2] U. E. Viesturs, M. Z. Kristapsons, and E. S. Levitans, 'Foam in microbiological processes', in *Microbes and Engineering Aspects*, vol. 21, Berlin, Heidelberg: Springer Berlin Heidelberg, 1982, pp. 169–224. doi: 10.1007/3-540-11019-4_8.

[3] T. Sasaki and S. Okazaki, 'Some remarks on foaming and defoaming', *Kolloid-Zeitschrift*, vol. 159, no. 1, pp. 11–15, Jul. 1958, doi: 10.1007/BF01520055.

[4] S. J. Routledge, 'BEYOND DE-FOAMING: THE EFFECTS OF ANTIFOAMS ON BIOPROCESS PRODUCTIVITY', *Computational and Structural Biotechnology Journal*, vol. 3, no. 4, p. e201210001, Oct. 2012, doi: 10.5936/csbj.201210014.

[5] '- Mechanical Methods for Defoaming', in *The Science of Defoaming*, 0 ed., CRC Press, 2016, pp. 416–457. doi: 10.1201/b15158-10.

[6] F. J. Lech, 'Foam properties of proteins, low molecular weight surfactants and their complexes', p. 130.

[7] D. Langevin, 'Influence of interfacial rheology on foam and emulsion properties', *Advances in Colloid and Interface Science*, vol. 88, no. 1–2, pp. 209–222, Dec. 2000, doi: 10.1016/S0001-8686(00)00045-2.

[8] P. J. Wilde, 'Interfaces: their role in foam and emulsion behaviour', *Current Opinion in Colloid & Interface Science*, vol. 5, no. 3–4, pp. 176–181, Jul. 2000, doi: 10.1016/S1359-0294(00)00056-X.

[9] P. A. Wierenga and H. Gruppen, 'New views on foams from protein solutions', *Current Opinion in Colloid & Interface Science*, vol. 15, no. 5, pp. 365–373, Oct. 2010, doi: 10.1016/j.cocis.2010.05.017.

[10] S. Tcholakova, N. D. Denkov, and A. Lips, 'Comparison of solid particles, globular proteins and surfactants as emulsifiers', *Phys. Chem. Chem. Phys.*, vol. 10, no. 12, p. 1608, 2008, doi: 10.1039/b715933c.

[11] A. Bhakta and E. Ruckenstein, 'Drainage and Coalescence in Standing Foams', *Journal of Colloid and Interface Science*, vol. 191, no. 1, pp. 184–201, Jul. 1997, doi: 10.1006/jcis.1997.4953.

[12] P. Wilde, A. Mackie, F. Husband, P. Gunning, and V. Morris, 'Proteins and emulsifiers at liquid interfaces', *Advances in Colloid and Interface Science*, vol. 108–109, pp. 63–71, May 2004, doi: 10.1016/j.cis.2003.10.011.

[13] M. B. J. Meinders and T. van Vliet, 'The role of interfacial rheological properties on Ostwald ripening in emulsions', *Advances in Colloid and Interface Science*, vol. 108–109, pp. 119–126, May 2004, doi: 10.1016/j.cis.2003.10.005.

[14] S. Tcholakova, Z. Mitrinova, K. Golemanov, N. D. Denkov, M. Vethamuthu, and K. P. Ananthapadmanabhan, 'Control of Ostwald Ripening by Using Surfactants with High Surface Modulus', *Langmuir*, vol. 27, no. 24, pp. 14807–14819, Dec. 2011, doi: 10.1021/la203952p.

[15] P. R. Garrett, *The Science of Defoaming: Theory, Experiment and Applications*, 0 ed. CRC Press, 2016. doi: 10.1201/b15158.

[16] P. R. Garrett, 'Defoaming: Antifoams and mechanical methods', *Current Opinion in Colloid & Interface Science*, vol. 20, no. 2, pp. 81–91, Apr. 2015, doi: 10.1016/j.cocis.2015.03.007.

[17] N. D. Denkov and K. G. Marinova, ‘Antifoam Effects of Solid Particles, Oil Drops and Oil—Solid Compounds in Aqueous Foams’, in *Colloidal Particles at Liquid Interfaces*, 1st ed., B. P. Binks and T. S. Horozov, Eds. Cambridge University Press, 2006, pp. 383–444. doi: 10.1017/CBO9780511536670.011.
[18] F. Delvigne and J. Lecomte, ‘Foam Formation and Control in Bioreactors’, in *Encyclopedia of Industrial Biotechnology*, Hoboken, NJ, USA: John Wiley & Sons, Inc., 2010, p. eib326. doi: 10.1002/9780470054581.eib326.
[19] N. S. Deshpande and M. Barigou, ‘Mechanical suppression of the dynamic foam head in bubble column reactors’, *Chemical Engineering and Processing: Process Intensification*, vol. 39, no. 3, pp. 207–217, May 2000, doi: 10.1016/S0255-2701(99)00079-3.
[20] N. S. Deshpande and M. Barigou, ‘Performance characteristics of novel mechanical foam breakers in a stirred tank reactor’, *J. Chem. Technol. Biotechnol.*, vol. 74, no. 10, pp. 979–987, Oct. 1999, doi: 10.1002/(SICI)1097-4660(199910)74:10<979::AID-JCTB139>3.0.CO;2-8.
[21] S. Gutwald and A. Mersmann, ‘Mechanical foam breaking - a physical model for impact effects with high speed rotors’, *Chem. Eng. Technol.*, vol. 20, no. 2, pp. 76–84, Feb. 1997, doi: 10.1002/ceat.270200203.
[22] S. Gutwald and A. Mersmann, ‘Bubble growth in secondary foams’, *Chem. Eng. Technol.*, vol. 20, no. 5, pp. 293–296, Jun. 1997, doi: 10.1002/ceat.270200502.
[23] ‘Foam breaking by high speed rotors’, *Chem. Eng. Technol.*, p. 11, 1990.
[24] A. G. Vetoshkin, ‘Modeling of Centrifugal Rotary Plate Foam Breakers’, vol. 37, no. 4, p. 6, 2003.
[25] S. Takesono, M. Onodera, K. Toda, M. Yoshida, K. Yamagiwa, and A. Ohkawa, ‘Improvement of foam breaking and oxygen-transfer performance in a stirred-tank fermenter’, *Bioprocess Biosyst Eng*, vol. 28, no. 4, pp. 235–242, Mar. 2006, doi: 10.1007/s00449-005-0028-x.
[26] J. Winterburn, ‘Sound Methods of Breaking Foam’, p. 71.
[27] J. A. Gallego-Juárez, G. Rodríguez, E. Riera, and A. Cardoni, ‘Ultrasonic defoaming and debubbling in food processing and other applications’, in *Power Ultrasonics*, Elsevier, 2015, pp. 793–814. doi: 10.1016/B978-1-78242-028-6.00026-0.
[28] G. Rodríguez *et al.*, ‘Experimental study of defoaming by air-borne power ultrasonic technology’, *Physics Procedia*, vol. 3, no. 1, pp. 135–139, Jan. 2010, doi: 10.1016/j.phpro.2010.01.019.
[29] G. Campolongo, ‘Biopharma PAT - Quality Attributes, Critical Process Parameters & Key Performance Indicators at the Bioreactor’, May 2018.
[30] C. Tietje and A. Brouder, Eds., ‘International Conference On Harmonisation Of Technical Requirements For Registration Of Pharmaceuticals For Human Use’, in *Handbook of Transnational Economic Governance Regimes*, Brill | Nijhoff, 2010, pp. 1041–1053. doi: 10.1163/ej.9789004163300.i-1081.897.
[31] S. J. Reyes, Y. Durocher, P. L. Pham, and O. Henry, ‘Modern Sensor Tools and Techniques for Monitoring, Controlling, and Improving Cell Culture Processes’, *Processes*, vol. 10, no. 2, p. 189, Jan. 2022, doi: 10.3390/pr10020189.
[32] H. Kagermann, W. Wahlster, and J. Helbig, ‘Securing the future of German manufacturing industry Recommendations for implementing the strategic initiative INDUSTRIE 4.0 Final report of the Industrie 4.0 Working Group.’ Accessed: Oct. 15, 2022. [Online]. Available: https://en.acatech.de/publication/recommendations-for-implementing-the-strategic-initiative-industrie-4-0-final-report-of-the-industrie-4-0-working-group/download-pdf?lang=en
[33] A. S. Mali, M. Jagtap, P. Karekar, and A. Maruška, ‘A BRIEF REVIEW ON PROCESS ANALYTICAL TECHNOLOGY (PAT)’, vol. 8, no. 1, p. 7.

[34] S. Beg, M. S. Hasnain, M. Rahman, and S. Swain, 'Introduction to Quality by Design (QbD): Fundamentals, Principles, and Applications', in *Pharmaceutical Quality by Design*, Elsevier, 2019, pp. 1–17. doi: 10.1016/B978-0-12-815799-2.00001-0.
[35] G. Gerzon, Y. Sheng, and M. Kirkitadze, 'Process Analytical Technologies – Advances in bioprocess integration and future perspectives', *Journal of Pharmaceutical and Biomedical Analysis*, vol. 207, p. 114379, Jan. 2022, doi: 10.1016/j.jpba.2021.114379.
[36] T. Wallocha and O. Popp, 'Off-Gas-Based Soft Sensor for Real-Time Monitoring of Biomass and Metabolism in Chinese Hamster Ovary Cell Continuous Processes in Single-Use Bioreactors', *Processes*, vol. 9, no. 11, p. 2073, Nov. 2021, doi: 10.3390/pr9112073.
[37] J. P. Carvell and J. E. Dowd, 'On-line Measurements and Control of Viable Cell Density in Cell Culture Manufacturing Processes using Radio-frequency Impedance', *Cytotechnology*, vol. 50, no. 1–3, pp. 35–48, Mar. 2006, doi: 10.1007/s10616-005-3974-x.
[38] C. Fung Shek and M. Betenbaugh, 'Taking the pulse of bioprocesses: at-line and in-line monitoring of mammalian cell cultures', *Current Opinion in Biotechnology*, vol. 71, pp. 191–197, Oct. 2021, doi: 10.1016/j.copbio.2021.08.007.
[39] Zhihong. Ge, A. G. Cavinato, and J. B. Callis, 'Noninvasive Spectroscopy for Monitoring Cell Density in a Fermentation Process', *Anal. Chem.*, vol. 66, no. 8, pp. 1354–1362, Apr. 1994, doi: 10.1021/ac00080a023.
[40] A. E. Cervera, N. Petersen, A. E. Lantz, A. Larsen, and K. V. Gernaey, 'Application of near-infrared spectroscopy for monitoring and control of cell culture and fermentation', *Biotechnol Progress*, p. NA-NA, 2009, doi: 10.1002/btpr.280.
[41] J. Alves-Rausch, R. Bienert, C. Grimm, and D. Bergmaier, 'Real time in-line monitoring of large scale Bacillus fermentations with near-infrared spectroscopy', *Journal of Biotechnology*, vol. 189, pp. 120–128, Nov. 2014, doi: 10.1016/j.jbiotec.2014.09.004.
[42] S. Bruder, M. Reifenrath, T. Thomik, E. Boles, and K. Herzog, 'Parallelised online biomass monitoring in shake flasks enables efficient strain and carbon source dependent growth characterisation of Saccharomyces cerevisiae', *Microb Cell Fact*, vol. 15, no. 1, p. 127, Dec. 2016, doi: 10.1186/s12934-016-0526-3.
[43] P. A. Lira-Parada, A. Tuveri, G. M. Seibold, and N. Bar, 'Comparison of noninvasive, in-situ and external monitoring of microbial growth in fed-batch cultivations in Corynebacterium glutamicum', *Biochemical Engineering Journal*, vol. 170, p. 107989, Jun. 2021, doi: 10.1016/j.bej.2021.107989.
[44] L. Chen *et al.*, 'The Genome of *Sulfolobus acidocaldarius* , a Model Organism of the Crenarchaeota', *J Bacteriol*, vol. 187, no. 14, pp. 4992–4999, Jul. 2005, doi: 10.1128/JB.187.14.4992-4999.2005.
[45] L.-J. Liu *et al.*, 'Physiology, Taxonomy, and Sulfur Metabolism of the Sulfolobales, an Order of Thermoacidophilic Archaea', *Frontiers in Microbiology*, vol. 12, 2021, doi: 10.3389/fmicb.2021.768283.
[46] K. Rastädter, D. J. Wurm, O. Spadiut, and J. Quehenberger, 'Physiological Characterization of *Sulfolobus acidocaldarius* in a Controlled Bioreactor Environment', *Int J Environ Res Public Health*, vol. 18, no. 11, Art. no. 11, Jan. 2021, doi: 10.3390/ijerph18115532.
[47] J. Quehenberger, A. Albersmeier, H. Glatzel, M. Hackl, J. Kalinowski, and O. Spadiut, 'A defined cultivation medium for *Sulfolobus acidocaldarius*', *J. Biotechnol.*, vol. 301, pp. 56–67, Aug. 2019, doi: 10.1016/j.jbiotec.2019.04.028.
[48] K. Rastädter, D. J. Wurm, O. Spadiut, and J. Quehenberger, 'The Cell Membrane of *Sulfolobus* spp.—Homeoviscous Adaption and Biotechnological Applications', *Int J Mol Sci*, vol. 21, no. 11, Art. no. 11, Jan. 2020, doi: 10.3390/ijms21113935.
[49] S. M. Jensen, V. L. Neesgaard, S. L. N. Skjoldbjerg, M. Brandl, C. S. Ejsing, and A. H. Treusch, 'The Effects of Temperature and Growth Phase on the Lipidomes of *Sulfolobus*

islandicus and *Sulfolobus tokodaii*', *Life*, vol. 5, no. 3, pp. 1539–1566, Aug. 2015, doi: 10.3390/life5031539.
[50] A. Ameri *et al.*, 'Formulation of a New Generation of Liposomes from Bacterial and Archeal Lipids', *Tropical Journal of Pharmaceutical Research*, vol. 15, no. 2, pp. 215-220–220, Jan. 2016, doi: 10.4314/tjpr.v15i2.1.
[51] G. B. Patel and G. D. Sprott, 'Archaeobacterial Ether Lipid Liposomes (Archaeosomes) as Novel Vaccine and Drug Delivery Systems', *Critical Reviews in Biotechnology*, vol. 19, no. 4, pp. 317–357, Jan. 1999, doi: 10.1080/0738-859991229170.
[52] J. Quehenberger, L. Shen, S.-V. Albers, B. Siebers, and O. Spadiut, '*Sulfolobus* - A Potential Key Organism in Future Biotechnology', *Front Microbiol*, vol. 8, p. 2474, 2017, doi: 10.3389/fmicb.2017.02474.
[53] L. Cerchia, M. Rossi, and A. Guagliardi, 'An archaeal chaperonin-based reactor for renaturation of denatured proteins', *Extremophiles*, vol. 4, no. 1, pp. 1–7, Feb. 2000, doi: 10.1007/s007920050001.
[54] S. Mohamad Pauzi, N. Ahmad, M. F. Yahya, and M. A. Arifin, 'The Effects of Antifoam Agent on Dead End Filtration Process', *IOP Conf. Ser.: Mater. Sci. Eng.*, vol. 358, p. 012038, May 2018, doi: 10.1088/1757-899X/358/1/012038.
[55] M. Barigou, 'Foam Rupture by Mechanical and Vibrational Methods', *Chem. Eng. Technol.*, vol. 24, no. 6, pp. 659–663, Jun. 2001, doi: 10.1002/1521-4125(200106)24:6<659::AID-CEAT659>3.0.CO;2-1.
[56] G. St-Pierre Lemieux, D. Groleau, and P. Proulx, 'Introduction on Foam and its Impact in Bioreactors', *Can J Biotech*, vol. 3, no. 2, pp. 143–157, Nov. 2019, doi: 10.24870/cjb.2019-000131.
[57] S. R. Lone, V. Kumar, J. R. Seay, D. L. Englert, and H. T. Hwang, 'Evaluation of Volumetric Mass Transfer Coefficient in a Stirred Tank Bioreactor Using Response Surface Methodology', *Environmental Progress*, p. 16.
[58] J. Aubin *et al.*, 'Effects of process conditions on foaming in stirred tanks', *th European Conference on Mixing*, p. 5, 2018.
[59] S. M. Stocks, M. Cooke, and P. J. Heggs, 'Inverted hollow spinning cone as a device for controlling foam and hold-up in pilot scale gassed agitated fermentation vessels', *Chemical Engineering Science*, vol. 60, no. 8–9, pp. 2231–2238, Apr. 2005, doi: 10.1016/j.ces.2004.11.016.
[60] K. Van't Riet, 'Review of Measuring Methods and Results in Nonviscous Gas-Liquid Mass Transfer in Stirred Vessels', *Ind. Eng. Chem. Proc. Des. Dev.*, vol. 18, no. 3, pp. 357–364, Jul. 1979, doi: 10.1021/i260071a001.
[61] J. Kager, 'kLa determination with dynamic oxygen transport equation'. 2022. Accessed: Sep. 22, 2022. [Online]. Available: https://gitlab.com/juliankager/kla_determination
[62] E. L. Paul, V. A. Atiemo-Obeng, and S. M. Kresta, Eds., *Handbook of industrial mixing: science and practice*. Hoboken, N.J: Wiley-Interscience, 2004.
[63] T. Kracík and T. Moucha, 'Ungassed power input prediction in stirred tank reactors', *Chem. Pap.*, vol. 76, no. 1, pp. 293–300, Jan. 2022, doi: 10.1007/s11696-021-01854-x.
[64] H. Zhu, A. W. Nienow, W. Bujalski, and M. J. H. Simmons, 'Mixing studies in a model aerated bioreactor equipped with an up- or a down-pumping "Elephant Ear" agitator: Power, hold-up and aerated flow field measurements', *Chemical Engineering Research and Design*, vol. 87, no. 3, pp. 307–317, Mar. 2009, doi: 10.1016/j.cherd.2008.08.013.
[65] M. Cooke, P. J. Heggs, A. Eaglesham, and D. Housley, 'Spinning Cones as Pumps, Degassers and Level Controllers in Mechanically Stirred Tanks', *Chemical Engineering Research and Design*, vol. 82, no. 6, pp. 719–729, Jun. 2004, doi: 10.1205/026387604774196000.

[66] Y. Bakri, P. Jacques, L. K. Shi, and P. Thonart, 'Influence of a New Axial Impeller on KLa and Xylanase Production by Penicillium canescens 10-10c', *Applied Biochemistry and Biotechnology*, p. 12, 2002.
[67] Y. Zhu, P. C. Bandopadhayay, and J. Wu, 'Measurement of Gas-Liquid Mass Transfer in an Agitated Vessel. A Comparison between Different Impellers.', *J. Chem. Eng. Japan / JCEJ*, vol. 34, no. 5, pp. 579–584, 2001, doi: 10.1252/jcej.34.579.
[68] J. Austerjost, R. Söldner, C. Edlund, J. Trygg, D. Pollard, and R. Sjögren, 'A Machine Vision Approach for Bioreactor Foam Sensing', *SLAS Technology*, vol. 26, no. 4, pp. 408–414, Aug. 2021, doi: 10.1177/24726303211008861.
[69] C. Slouka *et al.*, 'Low-Frequency Electrochemical Impedance Spectroscopy as a Monitoring Tool for Yeast Growth in Industrial Brewing Processes', *Chemosensors*, vol. 5, no. 3, p. 24, Aug. 2017, doi: 10.3390/chemosensors5030024.
[70] M. Lj. Napijalo, Z. Nikolić, J. DojčIloviĆ, M. M. Napijalo, and L. Novaković, 'TEMPERATURE DEPENDENCE OF ELECTRIC PERMITTIVITY OF LINEAR DIELECTRICS WITH IONIC AND POLAR COVALENT BONDS', *Journal of Physics and Chemistry of Solids*, vol. 59, no. 8, pp. 1255–1258, Aug. 1998, doi: 10.1016/S0022-3697(98)00049-3.
[71] C. Slouka *et al.*, 'A Novel Application for Low Frequency Electrochemical Impedance Spectroscopy as an Online Process Monitoring Tool for Viable Cell Concentrations', *Sensors*, vol. 16, no. 11, p. 1900, Nov. 2016, doi: 10.3390/s16111900.
[72] B. Moore, R. Sanford, and A. Zhang, 'Case study: The characterization and implementation of dielectric spectroscopy (biocapacitance) for process control in a commercial GMP CHO manufacturing process', *Biotechnol Progress*, vol. 35, no. 3, p. e2782, May 2019, doi: 10.1002/btpr.2782.
[73] Department of Applied Biotechnology and Food Science, Faculty of Chemical Technology and Biotechnology, Budapest University of Technology and Economics, Budafoki út 6-8., H-1111 Budapest, Hungary, B. Kiss, Á. Németh, and Department of Applied Biotechnology and Food Science, Faculty of Chemical Technology and Biotechnology, Budapest University of Technology and Economics, Budafoki út 6-8., H-1111 Budapest, Hungary, 'Application of a High Cell Density Capacitance Sensor to Different Microorganisms', *Period. Polytech. Chem. Eng.*, vol. 60, no. 4, pp. 290–297, Oct. 2016, doi: 10.3311/PPch.8824.